P-05-120

Forsmark site investigation

Borehole KFM06A

Uniaxial compression test of intact rock

Lars Jacobsson
SP Swedish National Testing and Research Institute

August 2005

Svensk Kärnbränslehantering AB
Swedish Nuclear Fuel
and Waste Management Co
Box 5864
SE-102 40 Stockholm Sweden
Tel 08-459 84 00
+46 8 459 84 00
Fax 08-661 57 19
+46 8 661 57 19

ISSN 1651-4416
SKB P-05-120

Forsmark site investigation

Borehole KFM06A

Uniaxial compression test of intact rock

Lars Jacobsson
SP Swedish National Testing and Research Institute

August 2005

Keywords: Rock mechanics, Uniaxial compression test, Elasticity parameters, Stress-strain curve, Post-failure behaviour, AP PF 400-04-121.

Abstract

Uniaxial compression tests, containing the complete loading response beyond compressive failure, so called post-failure tests, were carried out on 16 water saturated specimens of intact rock from borehole KFM06A in Forsmark. The cylindrical specimens were taken from drill cores at three depth levels ranging between 449–451 m, 483–503 m and 818–820 m. Moreover, the rock types were mapped as medium-grained granite (449–451 m), pegmatite (483–503 m) and granite-aplite (818–820 m). The elastic properties, represented by Young's modulus and the Poisson ratio, and the uniaxial compressive strength were deduced from these tests. The wet density of the specimens was determined before the mechanical tests. The specimens were photographed before and after the mechanical testing.

The measured densities for the water saturated specimens were in the range 2,610–2,670 kg/m^3 and had a mean value of 2,651 kg/m^3. The peak values of the axial compressive stress were in the range 157.0– 371.1 MPa with a mean value of 239.0 MPa. The elastic parameters were determined at load corresponding to 50% of the failure load, and it was found that Young's modulus was in the range 70.5–85.6 GPa with a mean value of 76.7 GPa, wheras the Poisson ratio was in the range of 0.19–0.35 with a mean value of 0.27. It was seen from the mechanical tests that the material in the specimens responded in a brittle way.

Sammanfattning

Enaxiella kompressionsprov med belastning upp till brott och efter brott, så kallade ”post-failure tests”, har genomförts på 16 stycken vattenmättade cylindriska provobjekt av intakt berg. Provobjekten har tagits från en borrkärna från borrhål KFM06A i Forsmark vid tre djupnivåer, 449–451 m, 483–503 m och 818–820 m. Bergarterna vid dessa nivåer var medelkornig granit (449–451 m), pegmatit (483–503 m) och granit-aplit (818–820 m). De elastiska egenskaperna, representerade av elasticitetsmodulen och Poissons tal, har bestämts ur försöken. Bergmaterialets densitet i vått tillstånd hos proverna mättes upp före de mekaniska proven. Provobjekten fotograferades före och efter de mekaniska proven.

Den uppmätta densiteten hos de vattenmättade proven var mellan 2 610–2 670 kg/m^3 med ett medelvärde på 2 651 kg/m^3. Toppvärdena för den kompressiva axiella spänningen låg mellan 157,0– 371,1 MPa med ett medelvärde på 239,0 MPa. De elastiska parametrarna bestämdes vid en last motsvarande 50 % av topplasten vilket gav en elasticitetsmodul på mellan 70,5–85,6 GPa med ett medelvärde på 76,7 GPa och Poissons tal mellan 0,19–0,35 med ett medelvärde på 0,27. Vid belastningsförsöken kunde man se att materialet i provobjekten hade ett sprött beteende.

Contents

1 Introduction

Uniaxial compression tests, with loading beyond the failure point into the post-failure regime, have been conducted on water-saturated specimens sampled from borehole KFM06A in Forsmark, see map in Figure 1-1. These tests belong to one of the activities performed as part of the site investigation in the Forsmark area managed by the Swedish Nuclear Fuel and Waste Management Co (SKB). The tests were carried out in the material and rock mechanics laboratories at the department of Building Technology and Mechanics at the Swedish National Testing and Research Institute (SP). All work was performed in accordance with the activity plan AP PF 400-04-121 (SKB internal controlling document) and was controlled by SP-QD 13.1 (SP internal quality document).

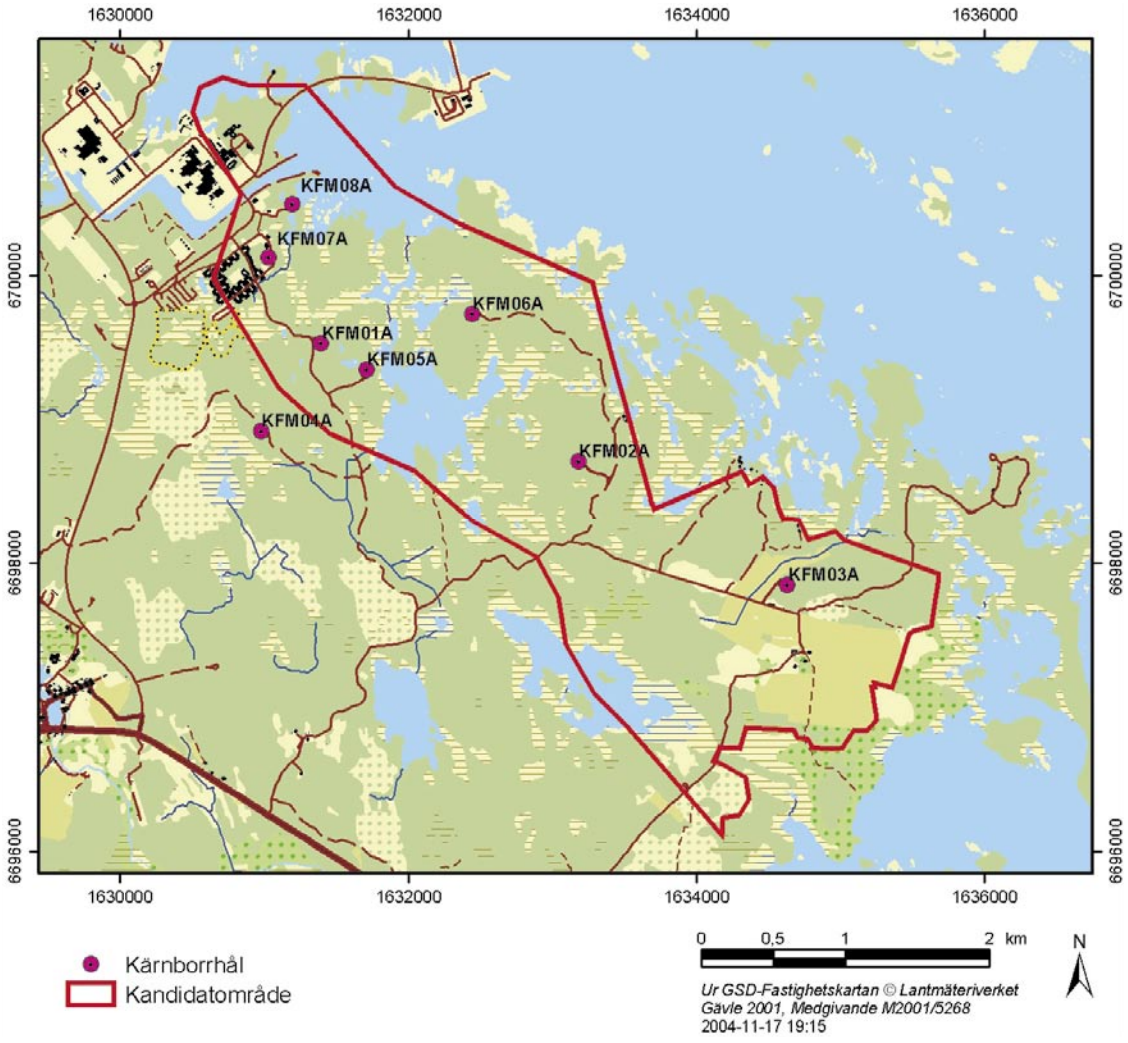

Figure 1-1. *Location of borehole KFM06A at the Forsmark site.*

SKB supplied SP with rock cores, and they arrived at SP in February 2005 and were tested during March 2005. Cylindrical specimens were cut from the cores and selected based on the preliminary core logging with the strategy to primarily investigate the properties of the dominant rock types. The method description SKB MD 190.001, version 2.0 (SKB internal controlling document) was followed for the sampling and for the uniaxial compression tests and the method description SKB MD 160.002, version 2.0 (SKB internal controlling document) was followed when the density was determined. As to the specimen preparation, the end surfaces on the specimens were grinded in order to comply with the required shape tolerances and then put in water and kept stored in water, for a minimum of 7 days, up to testing. This yields a water saturation, which is intended to resemble the in-situ moisture condition. The density was determined on each specimen and the uniaxial compression tests were carried out at this moisture condition. The specimens were photographed before and after the mechanical testing.

The uniaxial compression tests were carried out using radial strain as the feed-back signal in order to obtain the complete response in the post-failure regime on brittle specimens as is described in the method description SKB MD 190.001, version 2.0, and in the ISRM suggested method /1/. The axial ε_a and radial strain ε_r together with the axial stress σ_a were recorded during the test. The peak value of the axial compressive stress σ_c was determined at each test. Furthermore, two elasticity parameters, Young's modulus E and Poisson ratio v, were deduced from the tangent properties at 50% of the peak load. Diagrams with the volumetric and crack volumetric strain versus axial stress are reported. These diagrams can be used to determine crack initiation stress σ_i and the crack damage stress σ_d, cf /2, 3/.

2 Objective and scope

The purpose of the testing is to determine the uniaxial compressive strength and the elastic properties, represented by Young's modulus and the Poisson ratio, of cylindrical specimens of intact rock sampled from drill cores. Moreover, the specimens had a water content corresponding to the in-situ conditions. The loading was carried out into the post-failure regime in order to study the mechanical behaviour of the rock after cracking, thereby enabling determination of the brittleness and residual strength. The specimens originate from borehole KFM06A, which is inclined c 60° from the horizontal plane and has a drilling length of c 1,000 m.

The results from the tests are to be used in the site descriptive rock mechanics model, which will be established for the candidate area selected for site investigations at Forsmark.

3 Equipment

3.1 Specimen preparation and density measurement

A circular saw with a diamond blade was used to cut the specimens to their final lengths. The surfaces were then grinded after cutting in a grinding machine in order to achieve a high-quality surface for the axial loading that complies with the required tolerances. The measurements of the specimen dimensions were made with a sliding calliper. Furthermore, the tolerances were checked by means of a dial indicator and a stone face plate. The specimen preparation is carried out in accordance with ASTM 4543-01 /4/.

The specimens and the water were weighed using a scale weighing machine. A thermometer was used for the water temperature measurements. The calculated wet density was determined with an uncertainty of ± 4 kg/m^3.

3.2 Mechanical testing

The mechanical tests were carried out in a servo controlled testing machine specially designed for rock tests, see Figure 3-1. The system consists of a load frame, a hydraulic pump unit, a controller unit and various sensors. The communication with the controller unit is accomplished by means of special testing software running on a PC connected to the controller. The load frame has a high stiffness and a rapidly responding actuator, cf the ISRM suggested method /1/.

The stiffness of the various components of the loading chain in the load frame has been optimized in order to obtain a high total stiffness. This includes, the load frame, load cell, load platens and piston, as well as minimizing the amount of hydraulic oil in the cylinder. Furthermore, the sensors, the controller and the servo valve are rapidly responding components. The axial load is determined using a load cell, which has a maximum capacity of 1.5 MN. The uncertainty of the load measurement is less than 1%.

The axial and circumferential (radial) deformations of the rock specimens were measured. The rock deformation measurement systems are based on miniature LVDTs, which have a measurement range of +/– 2.5 mm. The relative error for the LVDTs are less than 0.6% within a 1 mm range for the axial deformation measurements and less than 1.3% within a 3 mm range for the circumferential deformation measurement. The LVDTs have been calibrated by means of a micrometer.

Two independent systems were used for the axial deformation measurement in order to obtain two comparative results. The first system (S1), see Figure 3-2, comprises two aluminium rings that are attached on the specimen placed at ¼ and ¾ of the specimen height. Two LVDTs mounted on the rings are used to measure the distance change between the rings on opposite sides of the specimen. As to the attachment, a rubber band made of a thin rubber hose with 0.5 mm thickness is first mounted on the specimen right under where the rings are to be mounted. The rings have three adjustable spring-loaded screws, each with a rounded tip pointing on the specimen with 120 degrees division. The screw tips are thus pressing on the rubber band. The second system (S2), see Figure 3-3, consists of two aluminium plates that are clamped around the circular loading platens of steel on top and on

bottom of the specimen. Two LVDTs, mounted on the plates, measure the distance change between these plates on opposite sides of the specimen at corresponding positions as for the first measurement system (S1).

The radial deformation was obtained by using a chain mounted around the specimen at mid-height, see Figures 3-2 and 3-3. The change of the chain-opening gap was measured by means of one LVDT and the circumferential, and thereby also the radial, deformation could be obtained. See Appendix A.

The specimens were photographed with a 4.0 Mega pixel digital camera at highest resolution and the photographs were stored in a jpeg-format.

Figure 3-1. *Rock testing system. From left: Digital controller unit, pressure cabinet (used for triaxial tests) and load frame. The PC with the test software (not shown in the picture) is placed on the left hand side of the controller unit.*

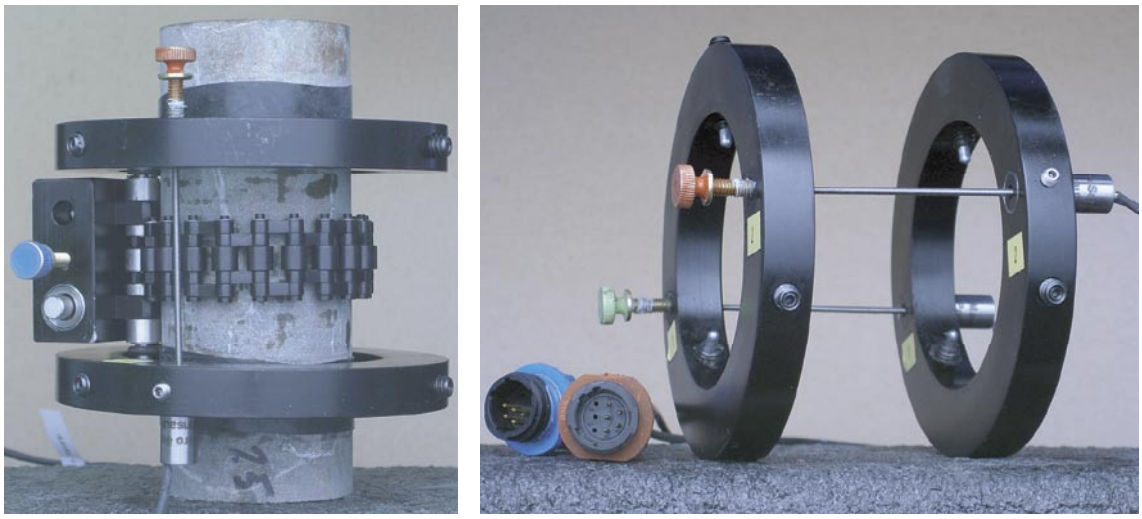

Figure 3-2. *Left: Specimen with two rubber bands. Devices for local axial and circumferential deformation measurements attached on the specimen. Right: Rings and LVDTs for local axial deformation measurement.*

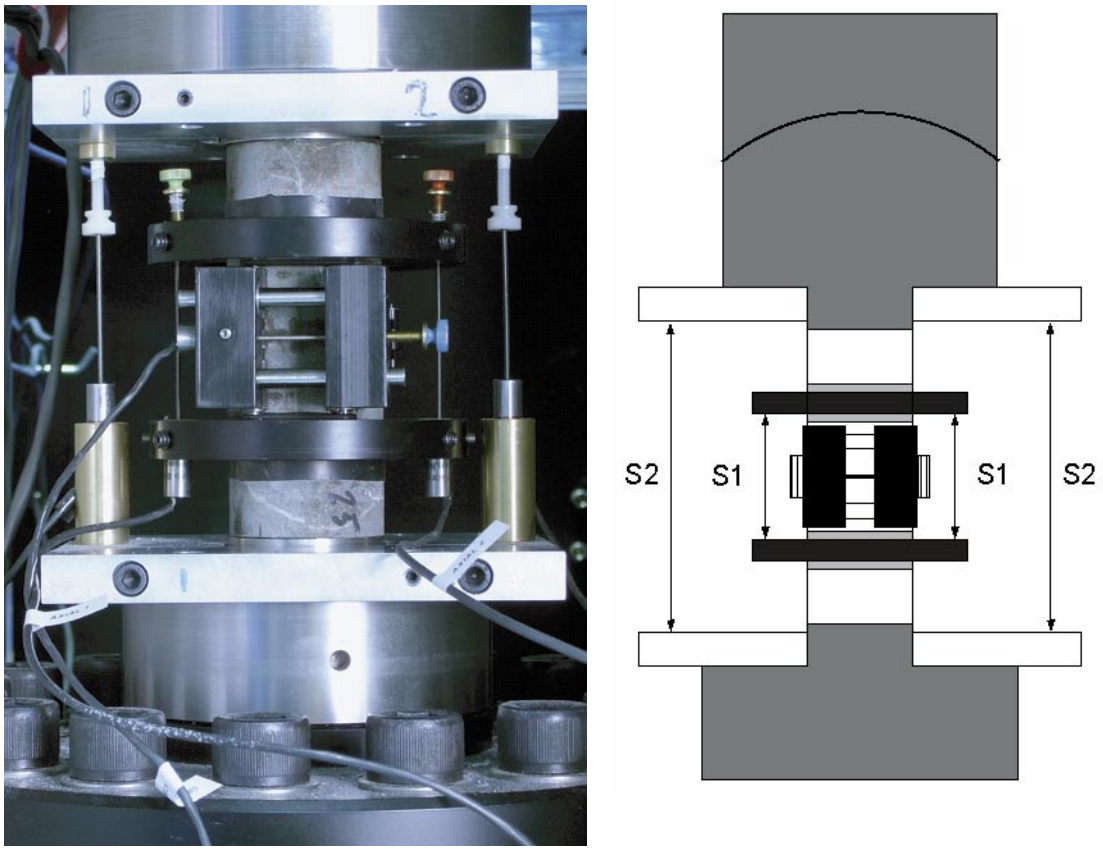

Figure 3-3. *Left: Specimen inserted between the loading platens. The two separate axial deformation measurement devices can be seen: system (S1) that measures the local axial deformation (rings) and system (S2) that measures the deformation between the aluminium plates (total deformation). Right: Principal sketch showing the two systems used for the axial deformation measurements.*

4 Execution

The water saturation and determination of the density of the wet specimens were made in compliance with the method description SKB MD 160.002, version 2.0 (SKB internal controlling document). This includes determination of density in accordance to ISRM /5/ and water saturation by SS-EN 13755 /6/. The uniaxial compression tests were carried out according to the method description SKB MD 190.001, version 2.0 (SKB internal controlling document). The test method is based on ISRM suggested method /1/.

4.1 Description of the samples

The rock type characterisation was made according to Stråhle (2001) /7/ using the SKB mapping system (Boremap). The identification marks, upper and lower sampling depth (Secup and Seclow) and the rock type are shown in Table 4-1.

Table 4-1. Specimen identification, sampling depth and rock type for all specimens (base on the overview mapping).

Identification	Secup (m)	Seclow (m)	Rock type
KFM06A-113-1	449.15	449.29	Medium-grained granite
KFM06A-113-2	449.29	449.43	Medium-grained granite
KFM06A-113-3	449.64	449.78	Medium-grained granite
KFM06A-113-4	449.78	449.92	Medium-grained granite
KFM06A-113-5	450.59	450.73	Medium-grained granite
KFM06A-113-6	450.73	450.87	Medium-grained granite
KFM06A-113-9	818.46	818.59	Granite-aplite (101058)
KFM06A-113-10	818.59	818.73	Granite-aplite (101058)
KFM06A-113-11	818.73	818.87	Granite-aplite (101058)
KFM06A-113-12	820.15	820.28	Granite-aplite (101058)
KFM06A-113-13	820.28	820.42	Granite-aplite (101058)
KFM06A-113-15	483.11	483.25	Pegmatite
KFM06A-113-16	483.25	483.39	Pegmatite
KFM06A-113-17	495.98	496.12	Pegmatite
KFM06A-113-18	496.12	496.26	Pegmatite
KFM06A-113-19	503.36	503.50	Pegmatite

4.2 Specimen preparation and density measurement

The temperature of the water was 24.5°C, which equals to a water density of 997.2 kg/m^3, when the determination of the wet density of the rock specimens was carried out. Further, the specimens had been stored for 10 days in water when the density was determined.

An overview of the procedure for specimen preparation is shown in the step-by step description in Table 4-2.

Table 4-2. Procedure for specimen preparation.

Step	Activity
1	The drill cores were marked where the specimens are to be taken.
2	The specimens were cut to the specified length according to markings and the cutting surfaces were grinded.
3	The tolerances were checked: parallel and perpendicular end surfaces, smooth and straight circumferential surface.
4	The diameter and height were measured three times each. The respective mean value determines the dimensions that are reported.
5	The specimens were then water saturated according to the method described in SKB MD 160.002, version 2.0, and were stored for minimum 7 days in water, whereupon the wet density was determined.

4.3 Mechanical testing

The specimens had been stored during 31–39 days in water when the uniaxial compression tests were carried out. The functionality of the testing system was checked, by performing tests on other cores with a similar rock type before the tests described in this report started. A check-list was filled in successively during the work in order to confirm that the different specified steps had been carried out. Moreover, comments were made upon observations made during the mechanical testing that are relevant for the interpretation of the results. The check-list form is an SP internal quality document.

An overview of the activities during the mechanical testing is given in the step-by step description in Table 4-3.

4.4 Data handling

The test results were exported as text files from the test software and stored in a file server on the SP computer network after each completed test. The main data processing, in which the elastic moduli were computed and the peak stress was determined, has been carried out in the program MATLAB /8/. Moreover, MATLAB was used to produce the diagrams shown in Section 5.1 and in Appendix B. The summary of results in Section 5.2 with tables containing mean value and standard deviation of the different parameters and diagrams were produced using MS Excel. MS Excel was also used for reporting data to the SICADA database.

Table 4-3. Step-by-step test procedure.

Step	Activity
1	Digital photos were taken on each specimen before the mechanical testing.
2	Devices for measuring axial and circumferential deformations were attached to the specimen.
3	The specimen was put in place and centred between the frame loading platens.
4	The core on each LVDT was adjusted by means of a set screw to the right initial position. This was done so that the optimal range of the LVDTs could be used for the deformation measurement.
5	The frame piston was brought down into contact with the specimen with a force corresponding to 0.6 MPa axial stress.
6	A load cycle with loading up to 5 MPa and unloading to 0.6 MPa was conducted in order to settle possible contact gaps in the spherical seat in the piston and between the rock specimen and the loading platens.
7	The centering was checked again.
8	The deformation measurement channels were zeroed in the test software.
9	The loading was started and the initial loading rate was set to a radial strain rate of –0.025%/min. The loading rate was increased after reaching the post-failure region. This was done in order to prevent the total time for the test to become too long.
10	The test was stopped either manually when the test had proceeded long enough to reveal the post-failure behaviour, or after severe cracking had occurred and it was judged that very little residual axial loading capacity was left in the specimen.
11	Digital photos were taken on each specimen after the mechanical testing.

4.5 Analyses and interpretation

As to the definition of the different results parameters we begin with the axial stress σ_a, which is defined as

$$\sigma_a = \frac{F}{A}$$

where F is the axial force acting on the specimen and A is the specimen cross section area. The peak value of the axial stress during a test is representing the uniaxial compressive strength σ_c in the results presentation.

The average value of the two axial displacement measurements on opposite sides of the specimen is used for the axial strain calculation, cf Figure 3-3. In the first measurement system (S1), the recorded deformation represents a local axial deformation δ_{local} between the points at ¼ and ¾ height. A local axial strain is defined as

$$\varepsilon_{a,local} = \delta_{local}/L_{local}$$

where L_{local} is the distance between the rings before loading.

In the second measurement system (S2), the recorded displacement corresponds to a total deformation that, in addition to total rock deformation, also contains the local deformations that occur in the contact between the rock and the loading plates, and further it also contains the deformation of the steel loading plates at each side of the specimen ends.

The average value of the two total deformation measurements on opposite sides of the specimen is defined as the total deformation δ_{total}. An axial strain based on the total deformation is defined as

$$\varepsilon_{a,total} = \delta_{total}/L_{total}$$

where L_{total} is the height of the rock specimen.

The radial deformation is measured by means of a chain mounted around the specimen at mid-height, cf Figures 3-2 and 3-3. The change of chain opening gap is measured by means of one LVDT. This measurement is used to compute the radial strain ε_r, see Appendix A. Moreover, the volumetric strain ε_{vol} is defined as

$$\varepsilon_{vol} = \varepsilon_a + 2\varepsilon_r$$

The stresses and the strains are defined as positive in compressive loading and deformation. The elasticity parameters are defined by the tangent Young's modulus E and tangent Poisson ratio ν as

$$E = \frac{\sigma_a(0.60\sigma_c) - \sigma_a(0.40\sigma_c)}{\varepsilon_a(0.60\sigma_c) - \varepsilon_a(0.40\sigma_c)}$$

$$\nu = -\frac{\varepsilon_r(0.60\sigma_c) - \varepsilon_r(0.40\sigma_c)}{\varepsilon_a(0.60\sigma_c) - \varepsilon_a(0.40\sigma_c)}$$

The tangents were evaluated with values corresponding to an axial load between 40% and 60% of the axial peak stress σ_c.

Two important observations can be made from the results:

(i) The results based on the total axial deformation measurement (S2) display a lower axial stiffness, i.e. a lower value on Young's modulus, than in the case when the results are based on the local axial deformation measurement (S1). This is due to the additional deformations from the contact interface between the rock specimen and the steel loading platens and also due to the deformation of the loading platens themselves.

(ii) It can be seen that the response differs qualitatively between the results obtained with the local axial deformation measurement system (S1) and the system that measures total axial deformation (S2). In some cases the post-peak response obtained with the local deformation measurement system seems not to be physically correct. This can be due to a number of reasons, e.g. that a crack caused a localized deformation, see Figure 4-1. Another explanation could be that the rings attached to the specimens have slightly slipped or moved, for example if a crack was formed nearby one of the attachment points.

It is reasonable to assume that results based on the local axial deformation measurement (S1) are fairly accurate up to the formation of the first macro-cracks or up to the peak load, but not after. However, the results obtained with the total axial deformation measurement (S2) seem to be qualitatively correct after failure. We will therefore report the results based on the total axial deformation measurement, but make a correction of those results as described below in order to get overall good results.

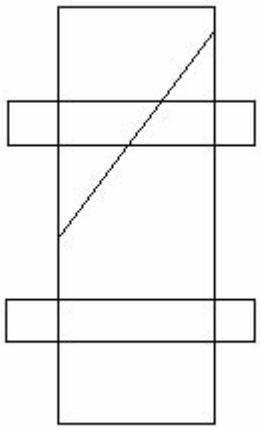

Figure 4-1. *Example of cracking that may cause results that are difficult to interpret with a local deformation measurement.*

The total axial deformation δ_{total} measured by (S2) is a summation of several deformations

$$\delta_{total} = \delta_{rock} + \delta_{system} \quad (1)$$

where

$$\delta_{system} = \delta_{interface} + \delta_{loading\ platens}$$

and δ_{rock} is the axial deformation of the whole rock specimen. Assume that the system deformation is proportional to the applied axial force F_a in the loading chain, i.e.

$$\delta_{system} = F_a/K_{system} \quad (2)$$

where K_{system} is the axial stiffness in the system (containing the interface between the rock and loading platens and the deformation of the loading platens). Combining (1) and (2) leads to

$$\delta_{rock} = \delta_{total} - F_a/K_{system} \quad (3)$$

where an expression of the axial deformation in the whole specimen is obtained. This can be viewed as a correction of the measurements made by system (S2). By using δ_{rock} to represent the axial deformation of the specimen that is based on a correction of the results of the total axial deformation will yield good results both in the loading range up to failure and also at loading after failure. However, it is noticed that K_{system} is not known and has to be determined.

It was previously suggested that the local axial deformation measurement represents the real rock deformation well up to the load where the macro-cracks form. Further, it is fair to assume that the axial deformation is homogenous at this part of the loading. Hence, we get

$$\delta_{rock} = \delta_{local} \cdot L_{total}/L_{local}$$

This yields representative values of the total rock deformation for the first part of the loading up to point where macro-cracking is taking place. By rewriting (2) we get

$$K_{system} = \frac{F_a}{\delta_{system}} \quad (4)$$

It is now possible to determine δ_{system} up to the threshold of macro-cracking. We will, however, compute the system stiffness based on the results between 40% and 60% of the axial peak stress σ_c. This means that Young's modulus and the Poisson ratio will take the same values both when the data from the local axial deformation measurement (S1) and when the data from corrected total axial deformation are used. This implies

$$K_{\text{system}} = \frac{F_a(0.60\sigma_c) - F_a(0.40\sigma_c)}{\delta_{\text{system}}(0.60\sigma_c) - \delta_{\text{system}}(0.40\sigma_c)} \tag{5}$$

where $\delta_{system} = \delta_{total} - \delta_{rock}$ according to (1). The results based on the correction according to (3) and (5) are presented in Section 5.1 whereas the original measured unprocessed data are reported in Appendix B.

A closure of present micro-cracks will take place initially during axial loading. Development of new micro cracks will start when the load is further increased and axial stress reaches the crack initiation stress σ_i. The crack growth at this stage is as stable as increased loading is required for further cracking. A transition from a development of micro-cracks to macro-cracks will take place when the axial load is further increased. At a certain stress level the crack growth becomes unstable. The stress level when this happens is denoted the crack damage stress σ_d, cf /2/. In order to determine the stress levels, we look at the volumetric strain.

By subtracting the elastic volumetric strain ε_{vol}^{e} from the total volumetric strain, a volumetric strain corresponding to the crack volume ε_{vol}^{cr} is obtained. This has been denoted calculated crack volumetric strain in the literature, cf /2, 3/. We have thus

$$\varepsilon_{vol}^{cr} = \varepsilon_{vol} - \varepsilon_{vol}^{e}$$

Assuming linear elasticity leads to

$$\varepsilon_{vol}^{cr} = \varepsilon_{vol} - \frac{1-2\nu}{E}\sigma_a$$

where $\sigma_r = 0$ was used. Experimental investigations have shown that the crack initiation stress σ_i coincides with the onset of increase of the calculated crack volume, cf /2, 3/. The same investigations also indicate that the crack damage stress σ_d can be defined as the axial stress at which the total volume starts to increase, i.e. when a dilatant behaviour is observed.

4.6 Nonconformities

The testing was conducted according to the method description with some deviations. The circumferential strains have been determined within a relative error of 1.5%, which is larger than what is specified in the ISRM-standard /1/. Further, double systems for measuring the axial deformation have been used, which is beyond the specifications in the method description. This was conducted as a development of the test method specially aimed for high-strength brittle rock. Moreover, the depth levels for specimens KFM06A-113-1 and KFM06A-113-16 to KFM06A-113-19 were not available from SKB mapping at the time of reporting the results.

One additional specimen was tested (KFM06A-113-1) compared to the number of specimens specified in the activity plan. This specimen was not photographed before the mechanical testing. Except for this, the activity plan was followed with no departures.

5 Results

The results of the individual specimens are presented in Section 5.1 and a summary of the results is given in Section 5.2. The reported parameters are based both on unprocessed raw data obtained from the testing and processed data and were reported to the SICADA database. These data together with the digital photographs of the individual specimens were handed over to SKB. The handling of the results follows SDP-508 (SKB internal controlling document) in general.

5.1 Description and presentation of the specimen

The cracking is shown in pictures taken of the specimens, and comments on observations that appeared during the testing are reported. The elasticity parameters have been evaluated by using the results from the local axial deformation measurements. The data from the adjusted total axial deformation measurements, cf Section 4.4, are shown in this section. Red rings are superposed on the graphs indicating every five minutes of the progress of testing.

Diagrams showing the data from both the local and the total axial deformation measurements, system (S1) and (S2) in Figure 3-3, and the computed individual values of K_{system} used at the data corrections are shown in Appendix B. The diagrams actual radial strain rates versus the test time are also presented in Appendix B. The results for the individual specimens are as follows:

Specimen ID: KFM06A-113-1

Before mechanical test

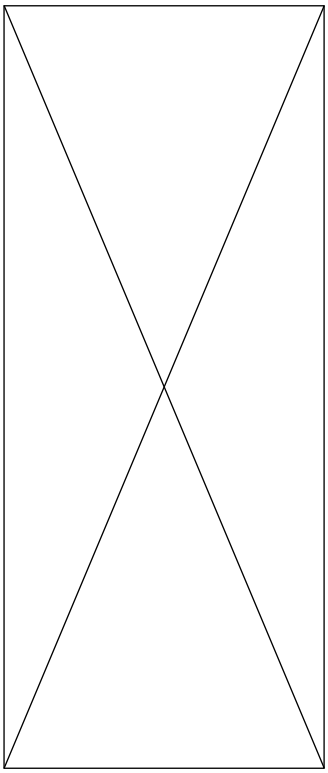

After mechanical test

Diameter (mm)	Height (mm)	Density (kg/m^3)
50.6	124.2	2,660

Comments Spalling on one side of the specimen in the longitudinal direction. The load started to oscillate when a crack was formed under the chain whereupon the test was stopped. No photo was taken on the specimen before the mechanical testing.

Specimen ID: KFM06A–113–01

Youngs Modulus (E):	74.7	[GPa]
Poisson Ratio (ν):	0.25	[–]
Axial peak stress (σ_c):	214.4	[MPa]

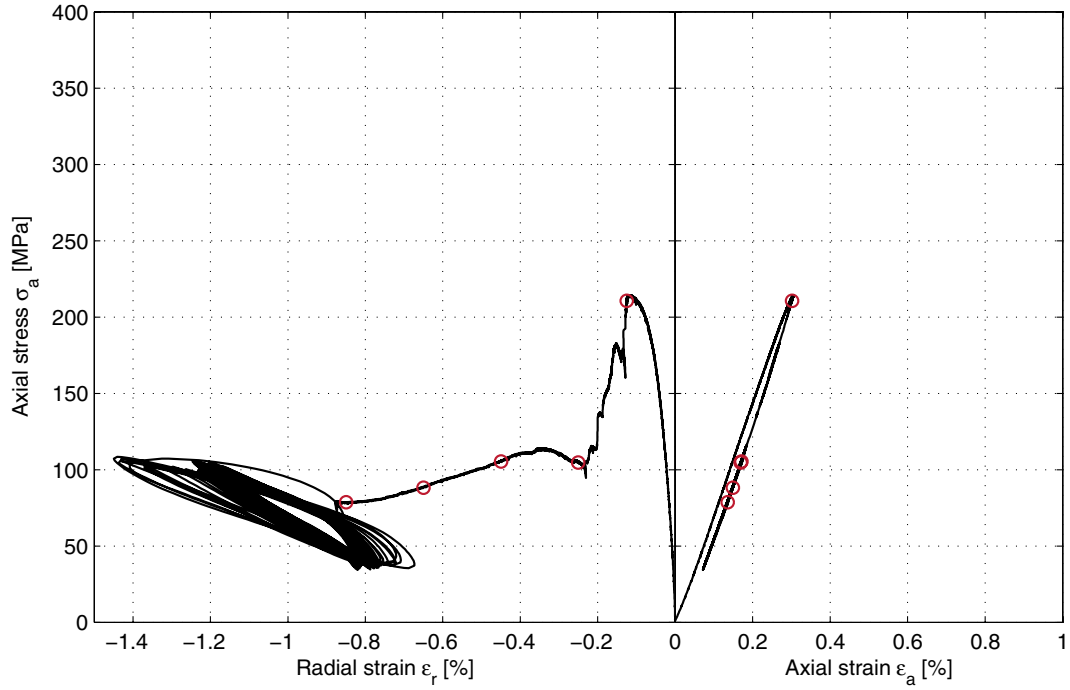

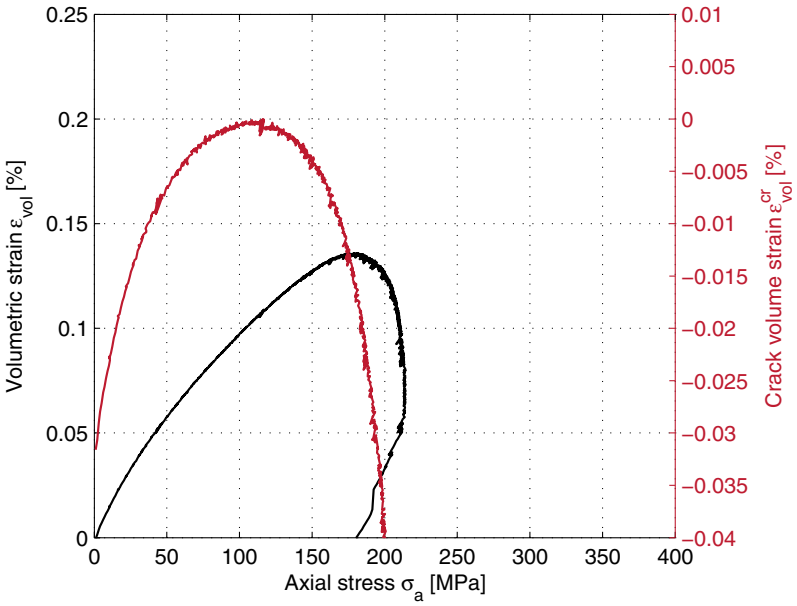

Specimen ID: KFM06A-113-2

Before mechanical test

After mechanical test

Diameter (mm)	Height (mm)	Density (kg/m^3)
50.6	124.2	2,670

Comments Spalling and vertical cracks are observed. The cracks seem to be partly oriented along the foliation direction.

Specimen ID: KFM06A−113−02

Youngs Modulus (E):	76.1	[GPa]
Poisson Ratio (ν):	0.23	[−]
Axial peak stress (σ_c):	157	[MPa]

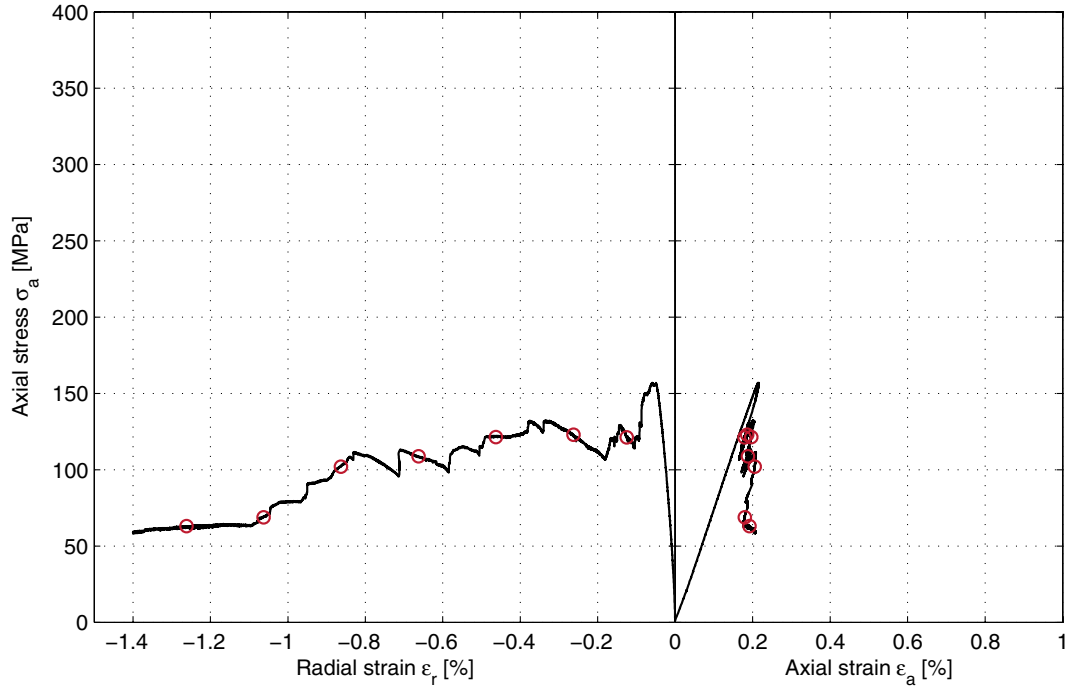

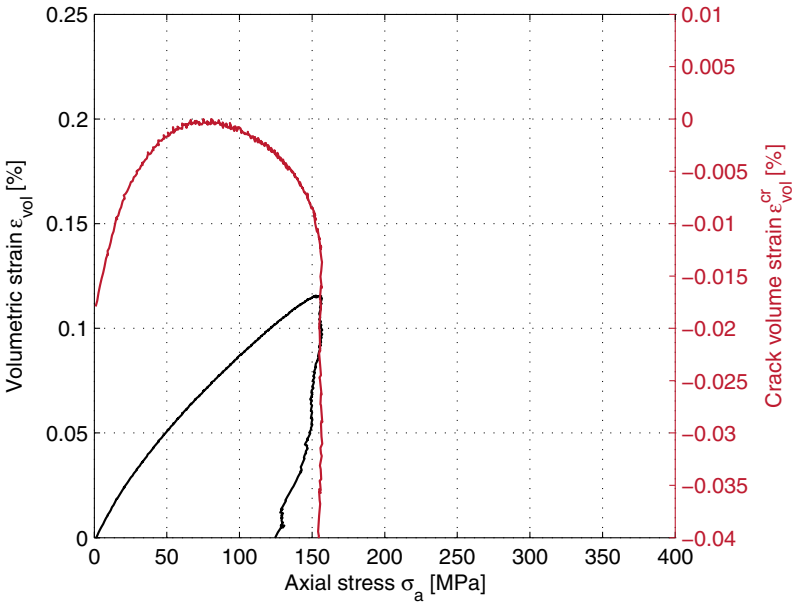

Specimen ID: KFM06A-113-3

Before mechanical test

After mechanical test

Diameter (mm)	Height (mm)	Density (kg/m^3)
50.6	124.2	2,670

Comments A band of another mineral transects the specimen, which also contains sealed cracks. A deep curved vertical failure partly follows the boundary between the minerals. This seems to have caused a reduced value of the compressive strength.

Specimen ID: KFM06A−113−03

Youngs Modulus (E):	76.7	[GPa]
Poisson Ratio (ν):	0.191	[−]
Axial peak stress (σ_c):	126.4	[MPa]

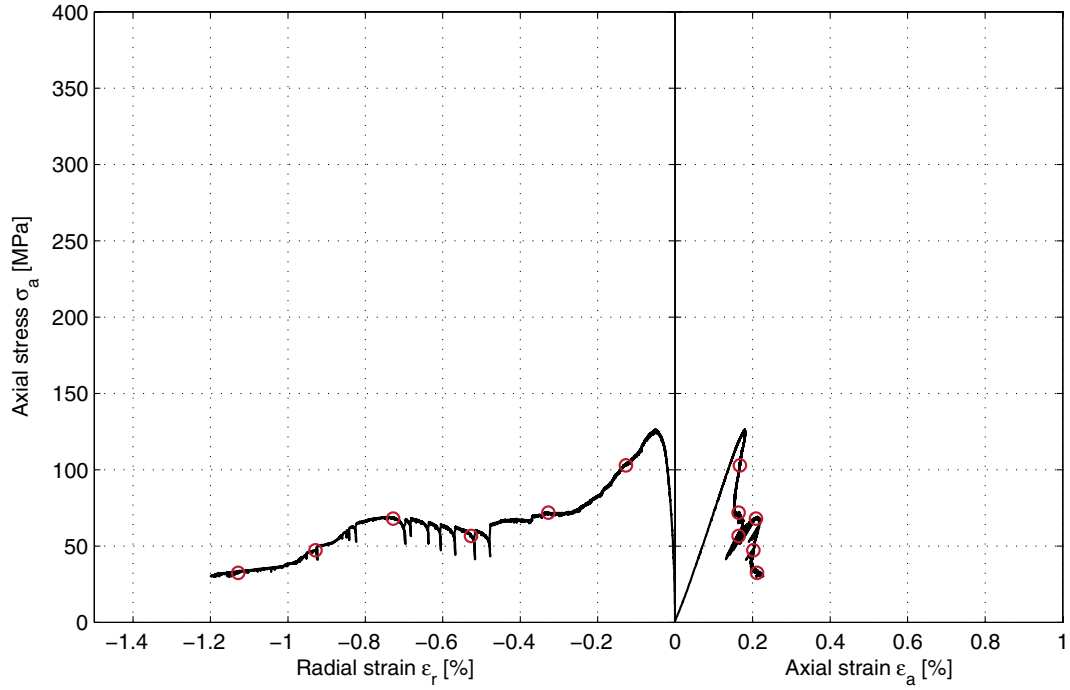

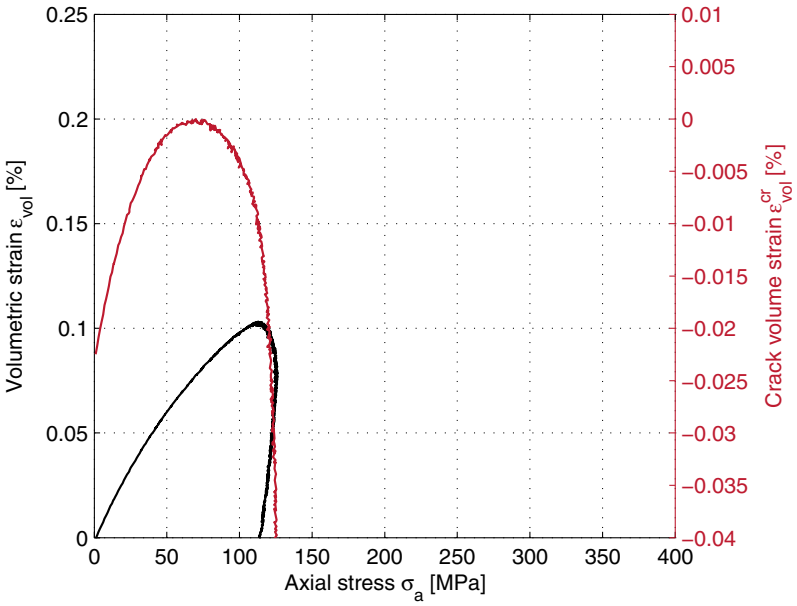

Specimen ID: KFM06A-113-4

Before mechanical test

After mechanical test

Diameter (mm)	Height (mm)	Density (kg/m^3)
50.6	124.6	2,670

Comments Deep spalling on one side and spalling on the opposite side that partly follows the foliation direction. The load started to oscillate due to the formation of cracks under the chain whereupon the test was stopped.

Specimen ID: KFM06A−113−04

Youngs Modulus (E):	74.3	[GPa]
Poisson Ratio (ν):	0.259	[−]
Axial peak stress (σ_c):	180.8	[MPa]

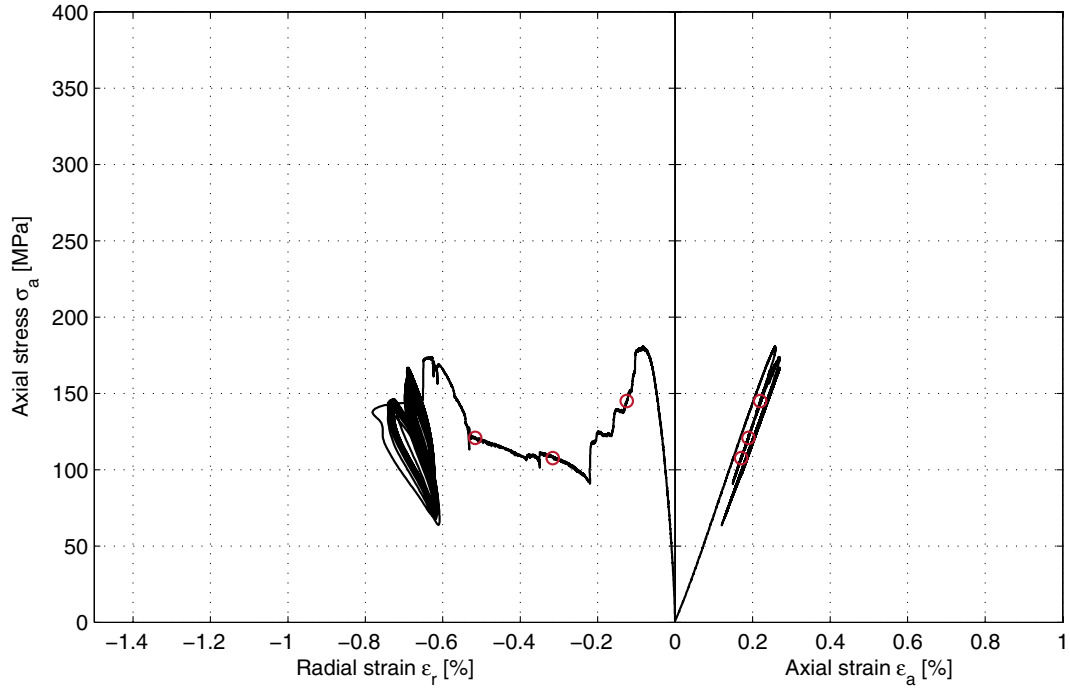

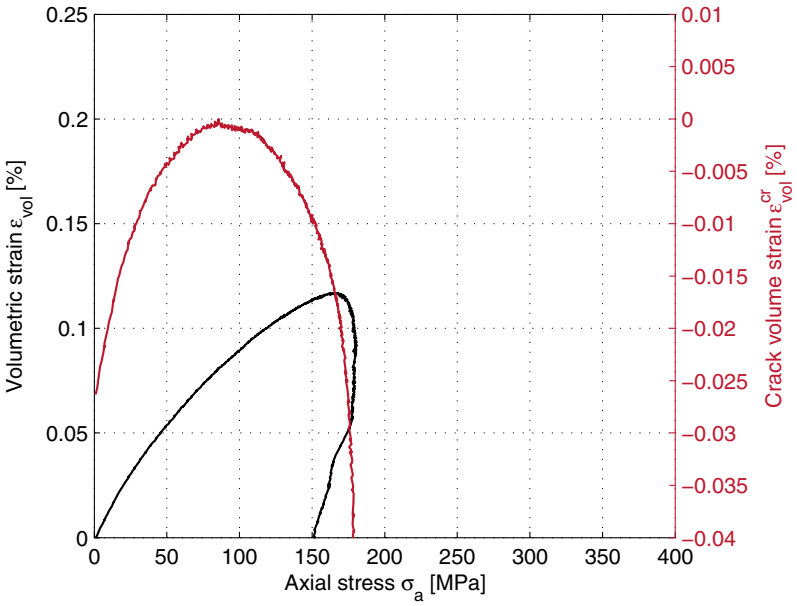

Specimen ID: KFM06A-113-5

Before mechanical test

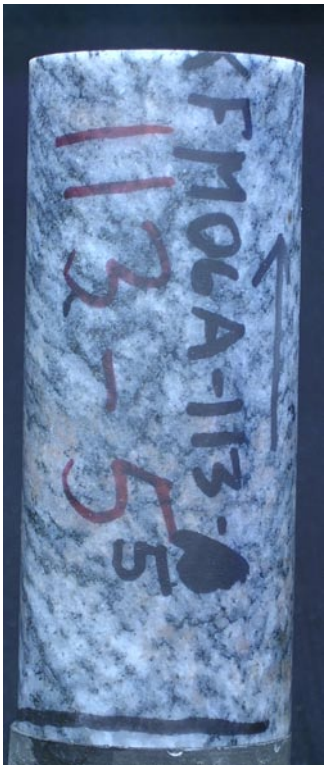

After mechanical test

Diameter (mm)	Height (mm)	Density (kg/m^3)
50.5	122.5	2,660

Comments Deep spalling on one side of the specimen in the longitudinal direction. The failure seems to partly follow the foliation direction. The load started to oscillate due to the formation of cracks under the chain whereupon the test was stopped.

Specimen ID: KFM06A−113−05

Youngs Modulus (E):	71.5	[GPa]
Poisson Ratio (ν):	0.3	[−]
Axial peak stress (σ_c):	194.8	[MPa]

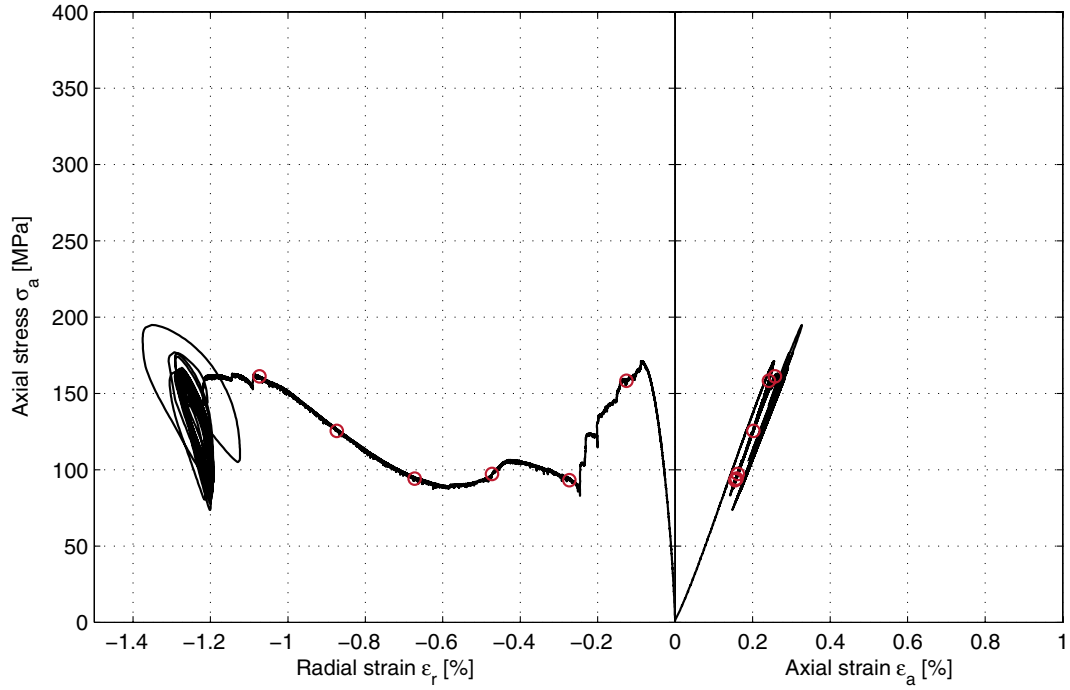

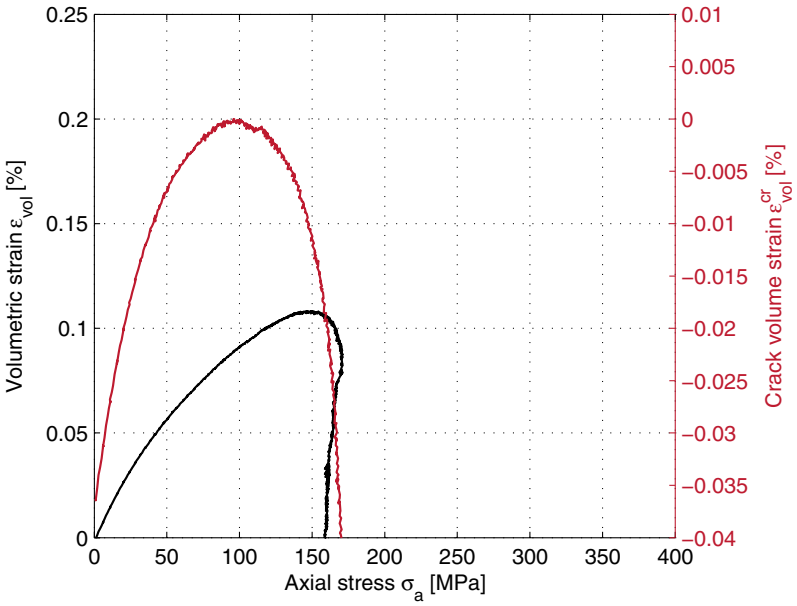

Specimen ID: KFM06A-113-6

Before mechanical test

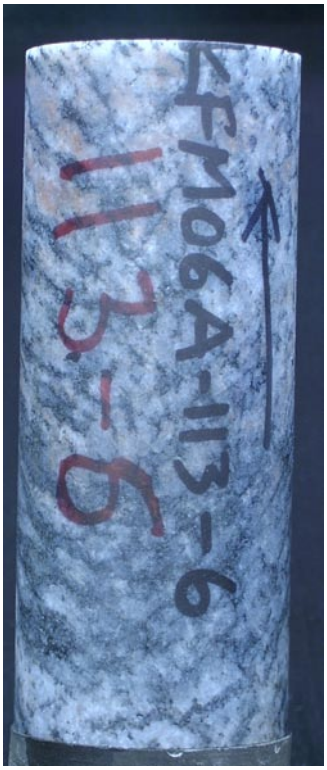

After mechanical test

Diameter (mm)	Height (mm)	Density (kg/m^3)
50.5	124.2	2,670

Comments Deep spalling on one side of the specimen in the longitudinal direction.

Specimen ID: KFM06A−113−06

Youngs Modulus (E):	70.5	[GPa]
Poisson Ratio (ν):	0.293	[−]
Axial peak stress (σ_c):	180.4	[MPa]

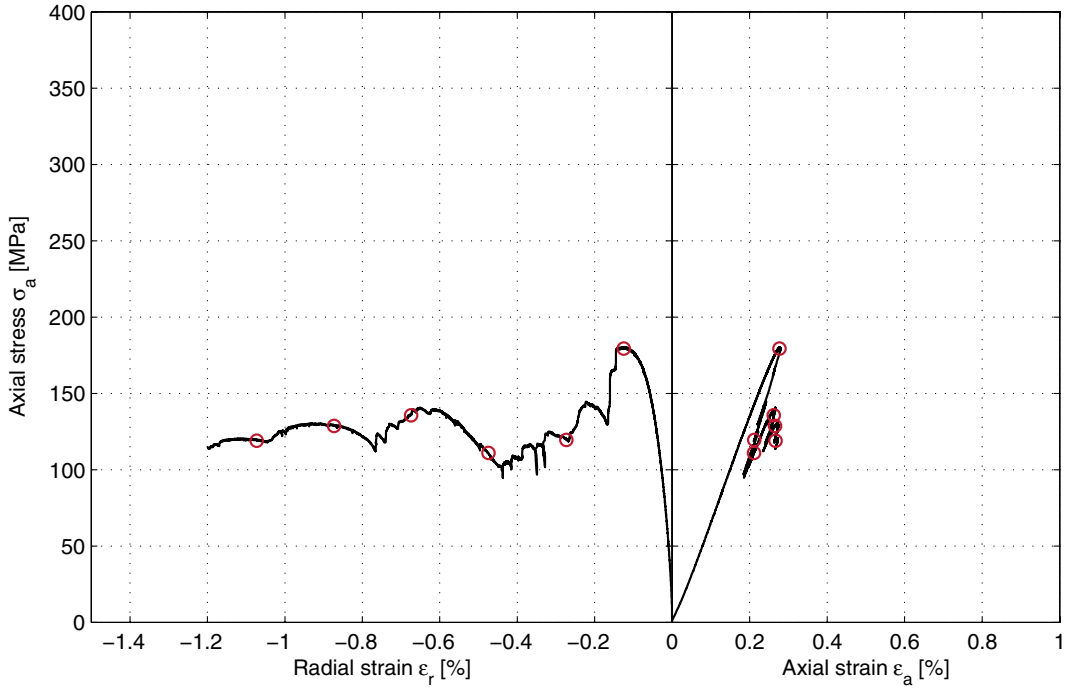

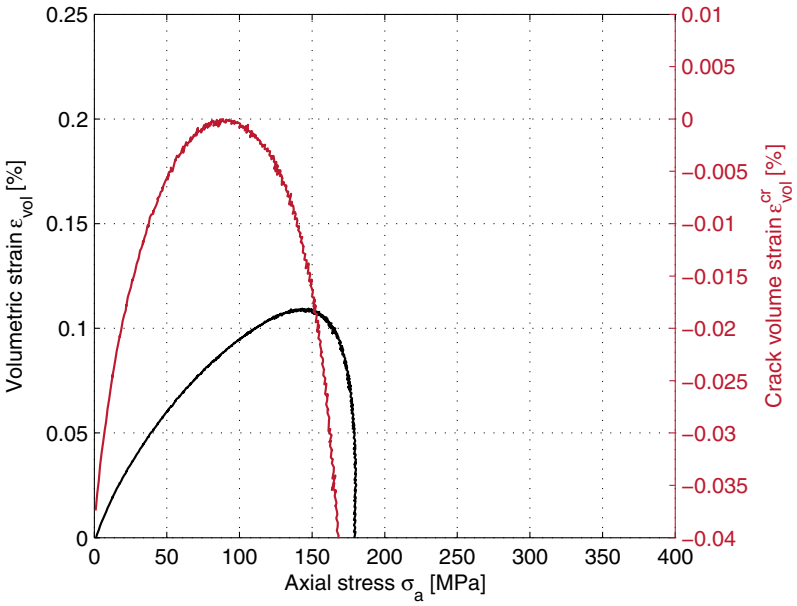

Specimen ID: KFM06A-113-9

Before mechanical test

After mechanical test

Diameter (mm)	Height (mm)	Density (kg/m^3)
50.5	125.1	2,660

Comments Spalling on one side of the specimen in the longitudinal direction. The load started to oscillate due to the formation of cracks under the chain whereupon the test was stopped.

Specimen ID: KFM06A–113–09

Youngs Modulus (E):	79.6	[GPa]
Poisson Ratio (ν):	0.247	[–]
Axial peak stress (σ_c):	229	[MPa]

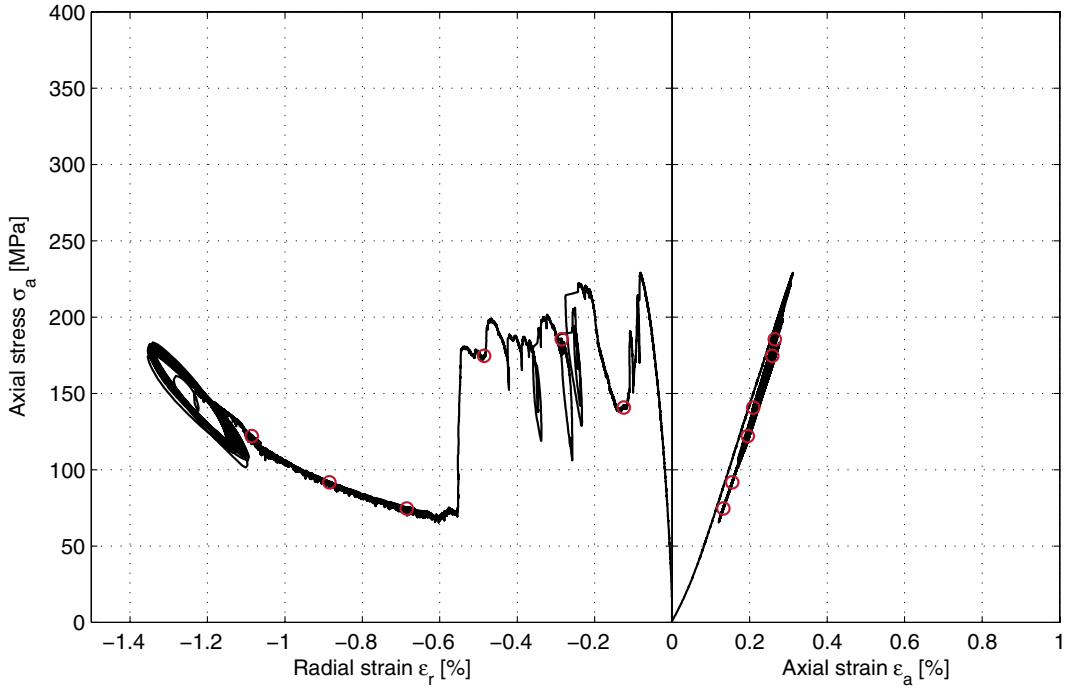

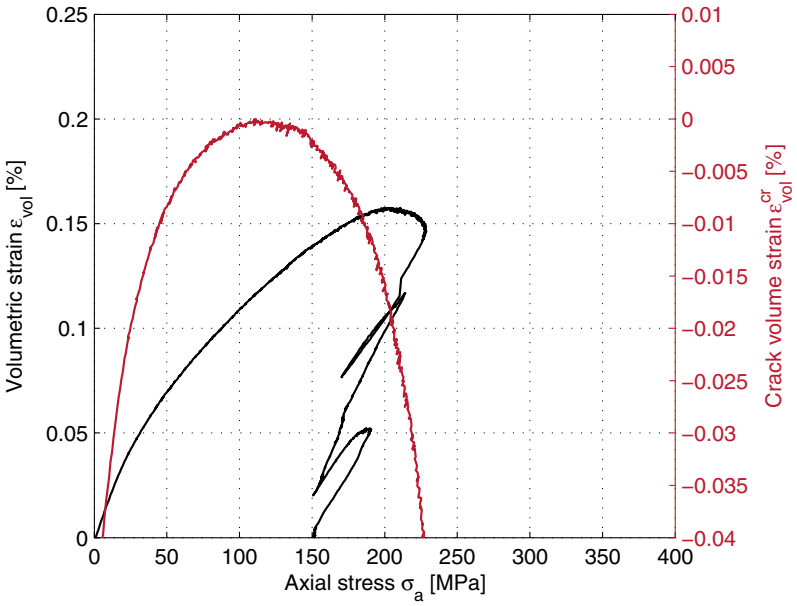

Specimen ID: KFM06A-113-10

Before mechanical test

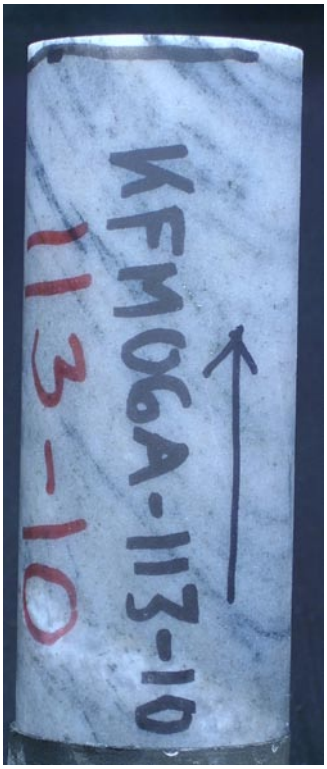

After mechanical test

Diameter (mm)	Height (mm)	Density (kg/m^3)
50.5	125.1	2,650

Comments Spalling on one side of the specimen in the longitudinal direction. Lots of crack noise was heard during the successive crack development.

Specimen ID: KFM06A–113–10

Youngs Modulus (E):	80.8	[GPa]
Poisson Ratio (ν):	0.306	[–]
Axial peak stress (σ_c):	371.1	[MPa]

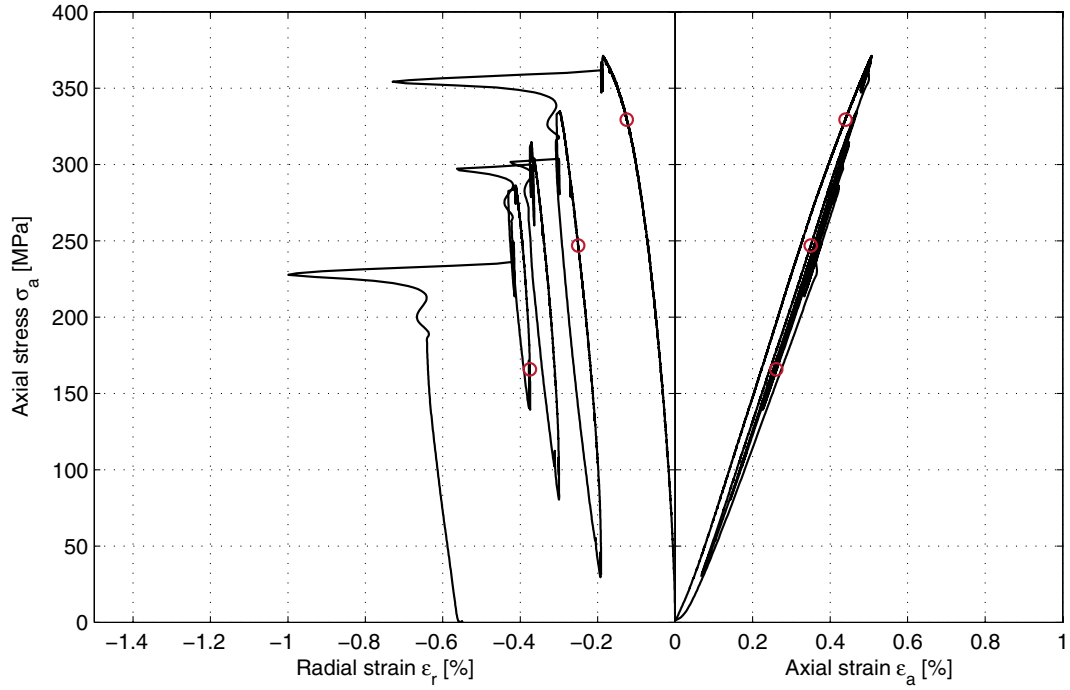

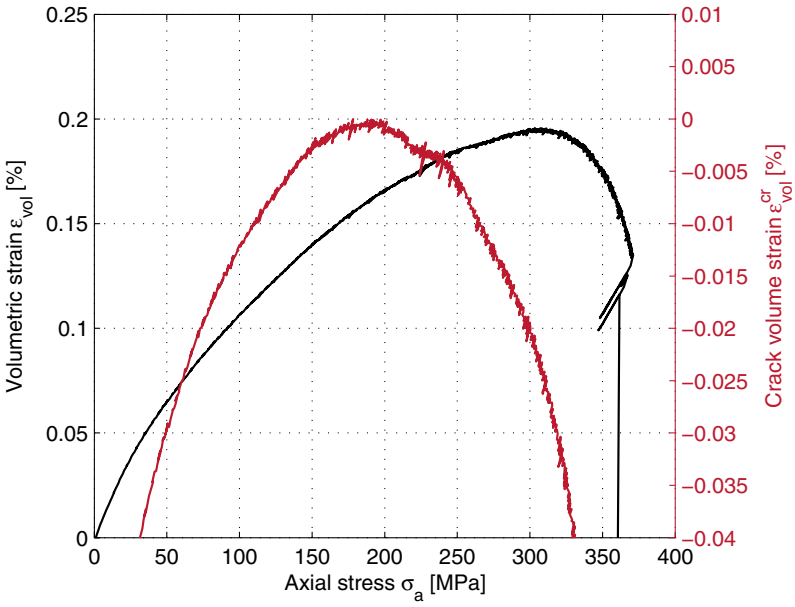

Specimen ID: KFM06A-113-11

Before mechanical test

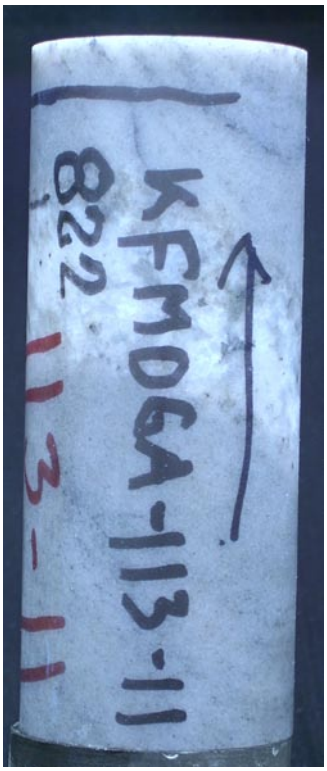

After mechanical test

Diameter (mm)	Height (mm)	Density (kg/m^3)
50.5	125.1	2,650

Comments Spalling and vertical failure guided by the foliation direction. Lots of crack noise was heard during the successive crack development. Short load oscillation during the test, but was stabilized and a sudden failure in the end of the test.

Specimen ID: KFM06A–113–11

Youngs Modulus (E):	85.6	[GPa]
Poisson Ratio (ν):	0.279	[–]
Axial peak stress (σ_c):	309.1	[MPa]

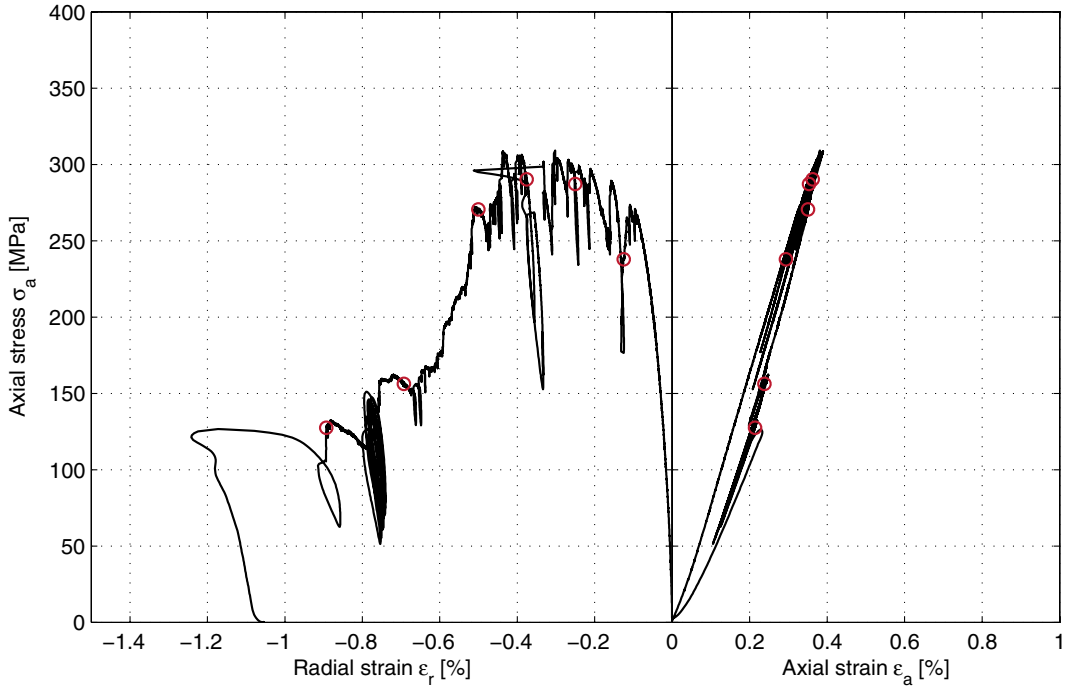

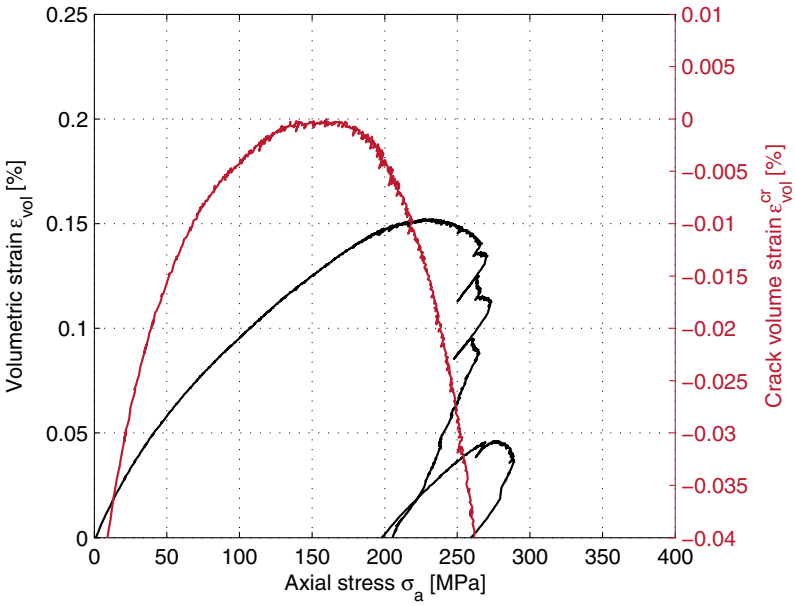

Specimen ID: KFM06A-113-12

Before mechanical test

After mechanical test

Diameter (mm)	Height (mm)	Density (kg/m^3)
50.6	122.7	2,660

Comments Spalling on one side of the specimen in the longitudinal direction that follows the foliation. Lots of crack noise was heard during the successive crack development. A sudden radial deformation due to cracking caused a complete unloading whereupon the test was ended.

Specimen ID: KFM06A−113−12

Youngs Modulus (E):	81.7	[GPa]
Poisson Ratio (ν):	0.255	[−]
Axial peak stress (σ_c):	357.7	[MPa]

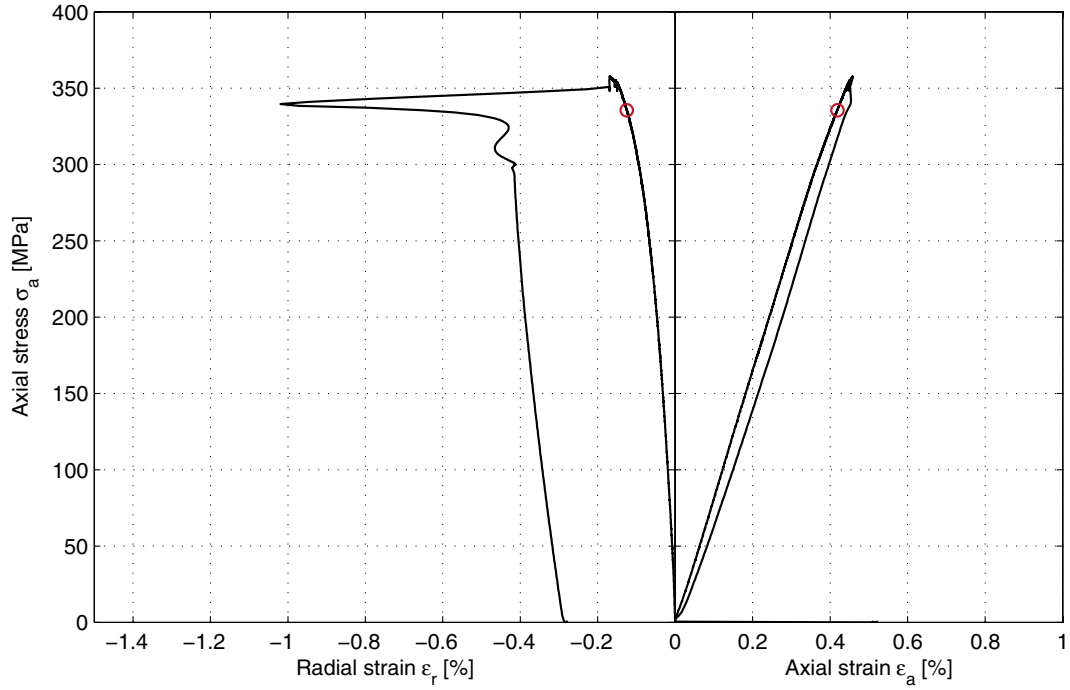

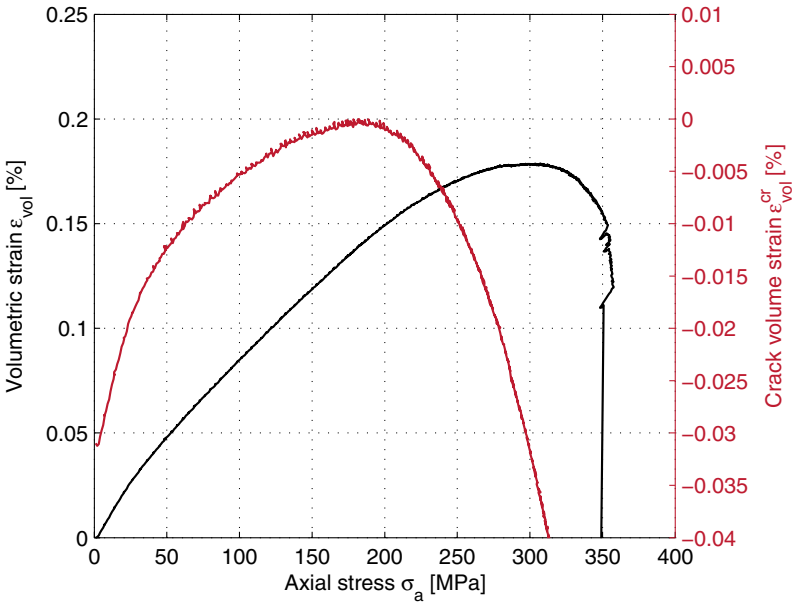

Specimen ID: KFM06A-113-13

Before mechanical test

After mechanical test

Diameter (mm)	Height (mm)	Density (kg/m^3)
50.6	125.1	2,660

Comments Spalling on one side of the specimen in the longitudinal direction that follows the foliation. A sudden radial deformation due to cracking caused a complete unloading whereupon the test was ended.

Specimen ID: KFM06A−113−13

Youngs Modulus (E):	85.6	[GPa]
Poisson Ratio (ν):	0.251	[−]
Axial peak stress (σ_c):	282.4	[MPa]

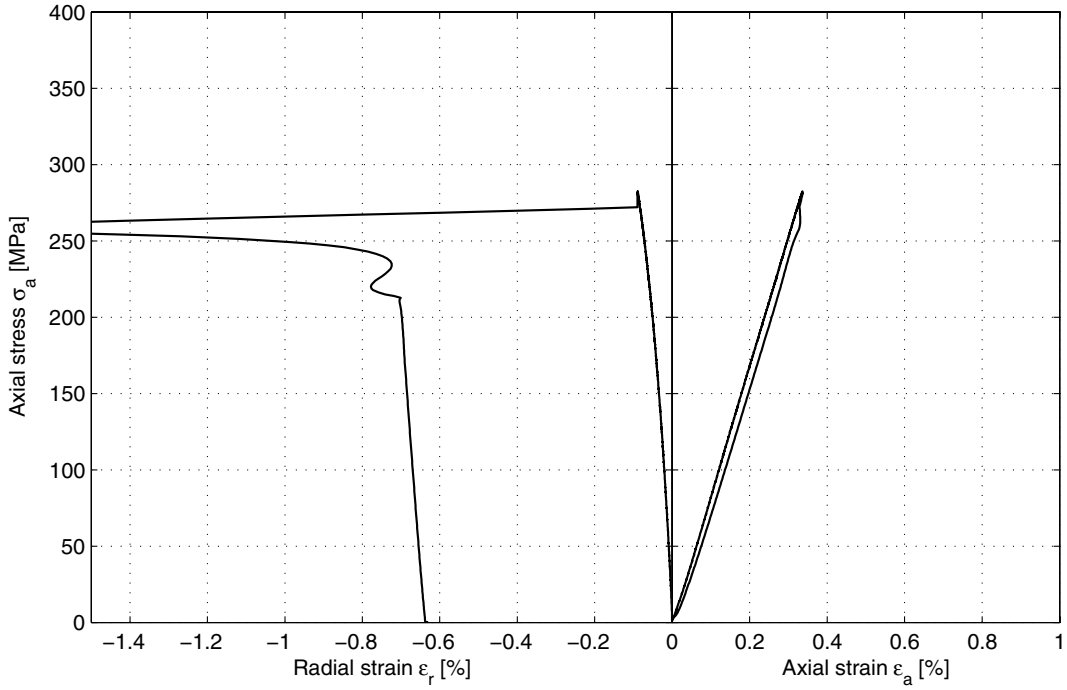

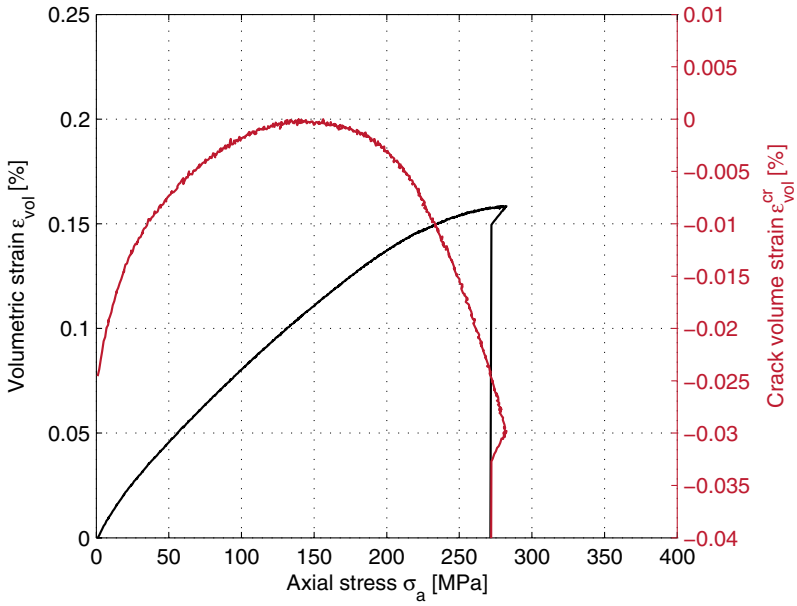

Specimen ID: KFM06A-113-15

Before mechanical test

After mechanical test

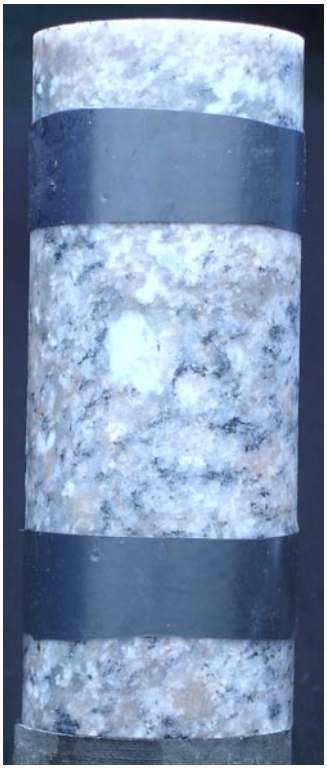

Diameter (mm)	Height (mm)	Density (kg/m^3)
50.4	127.7	2,620

Comments Spalling on one side of the specimen in the longitudinal direction. The load started to oscillate when a crack was formed under the chain whereupon the test was stopped.

Specimen ID: KFM06A−113−15

Youngs Modulus (E):	71.2	[GPa]
Poisson Ratio (ν):	0.297	[−]
Axial peak stress (σ_c):	232	[MPa]

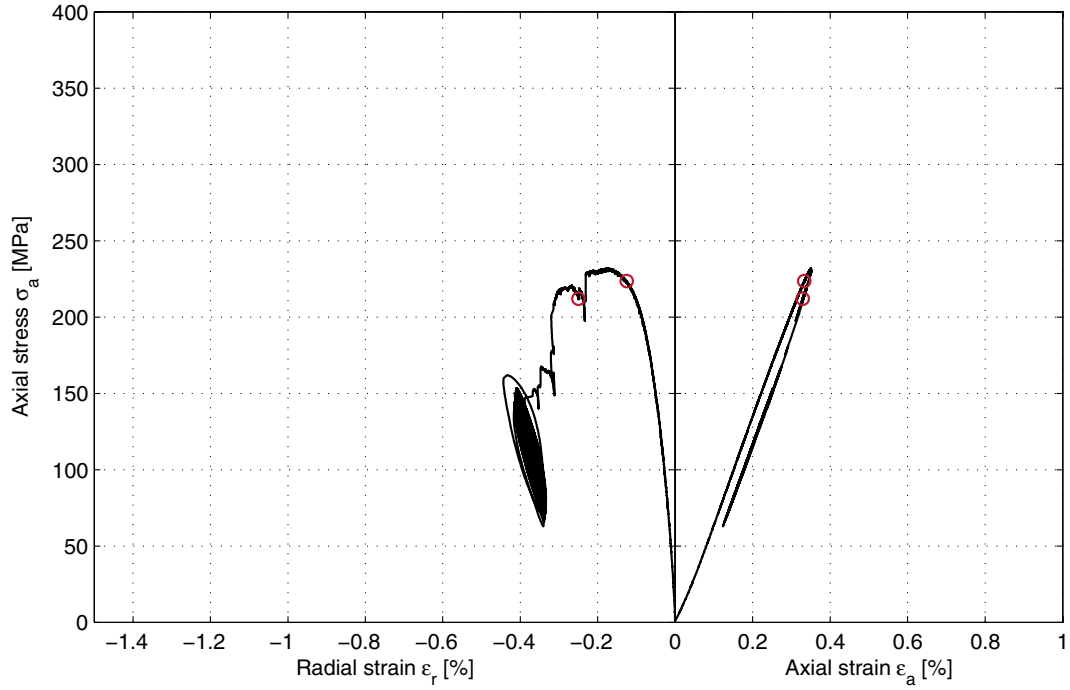

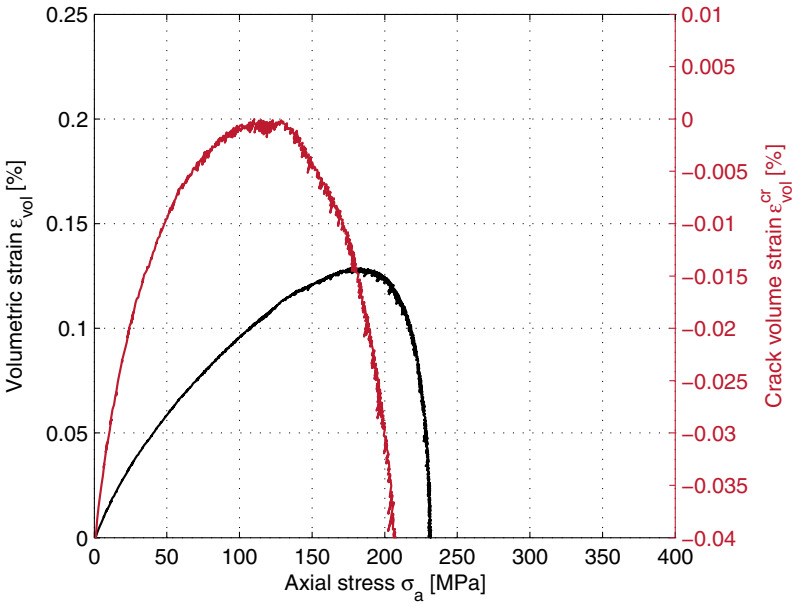

Specimen ID: KFM06A-113-16

Before mechanical test

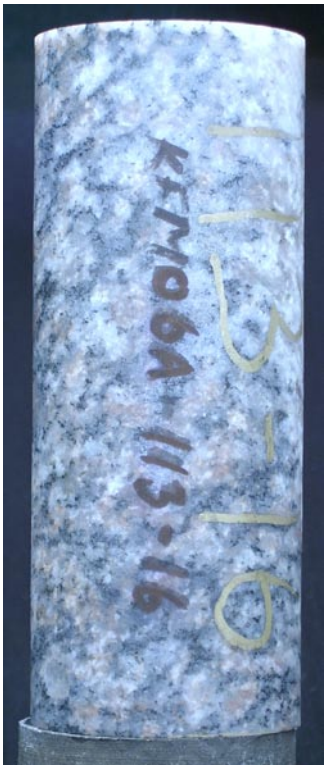

After mechanical test

Diameter (mm)	Height (mm)	Density (kg/m^3)
50.4	127.7	2,630

Comments Spalling on one side of the specimen in the longitudinal direction.

Specimen ID: KFM06A−113−16

Youngs Modulus (E):	72.1	[GPa]
Poisson Ratio (ν):	0.268	[−]
Axial peak stress (σ_c):	213.5	[MPa]

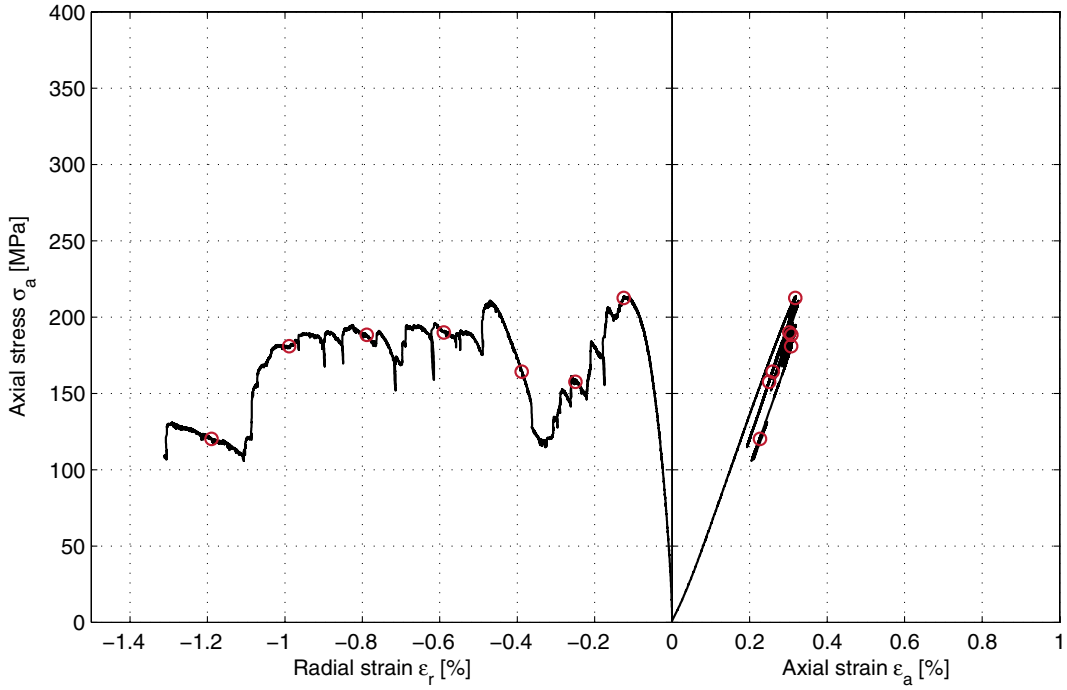

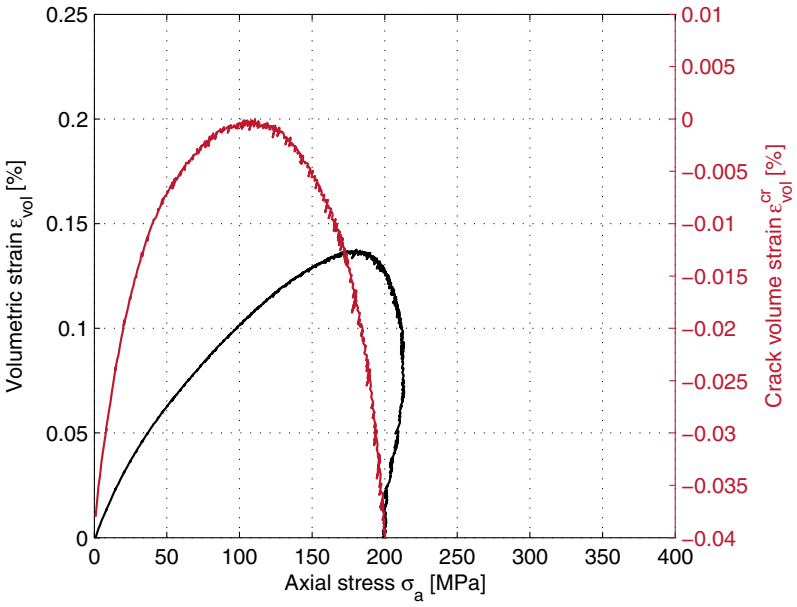

Specimen ID: KFM06A-113-17

Before mechanical test

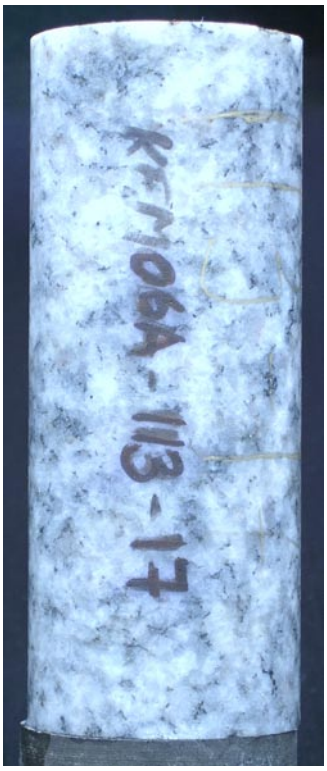

After mechanical test

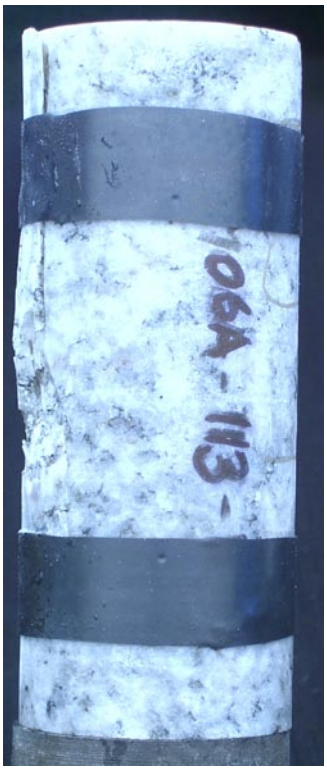

Diameter (mm)	Height (mm)	Density (kg/m^3)
50.7	127.7	2,640

Comments Spalling on one side of the specimen in the longitudinal direction.
A sudden radial deformation due to cracking caused a complete unloading whereupon the test was ended.

Specimen ID: KFM06A−113−17

Youngs Modulus (E):	79.8	[GPa]
Poisson Ratio (ν):	0.302	[−]
Axial peak stress (σ_c):	235.6	[MPa]

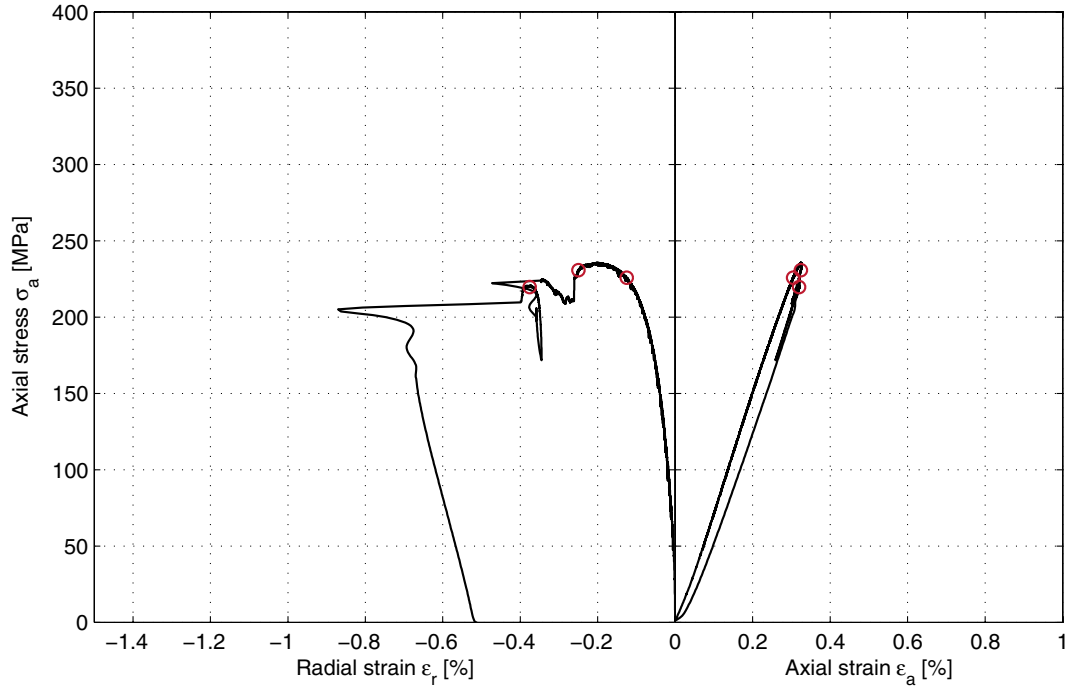

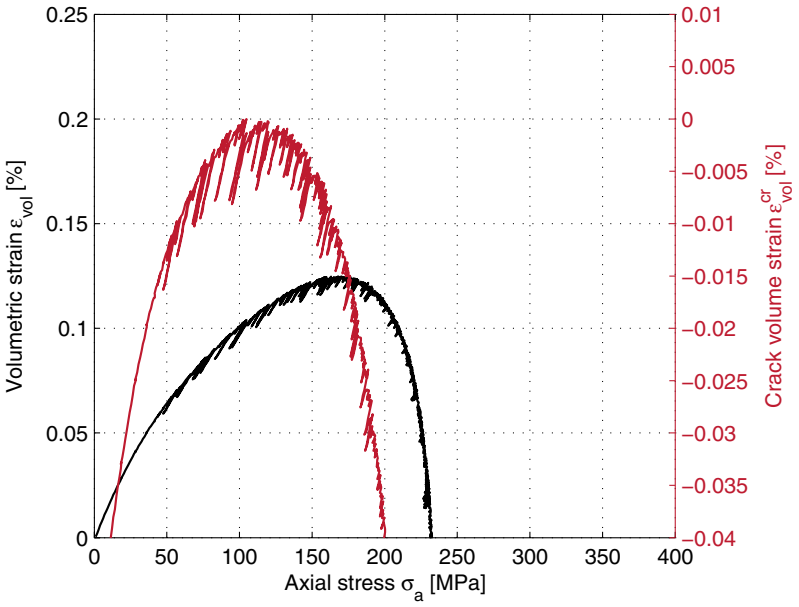

Specimen ID: KFM06A-113-18

Before mechanical test

After mechanical test

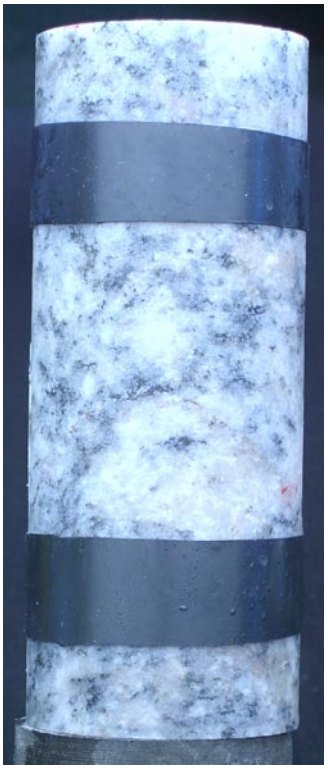

Diameter (mm)	Height (mm)	Density (kg/m^3)
50.7	127.7	2,640

Comments Spalling on one side of the specimen in the longitudinal direction. The load started to oscillate when a crack was formed under the chain whereupon the test was stopped.

Specimen ID: KFM06A−113−18

Youngs Modulus (E):	75.1	[GPa]
Poisson Ratio (ν):	0.258	[−]
Axial peak stress (σ_c):	192.1	[MPa]

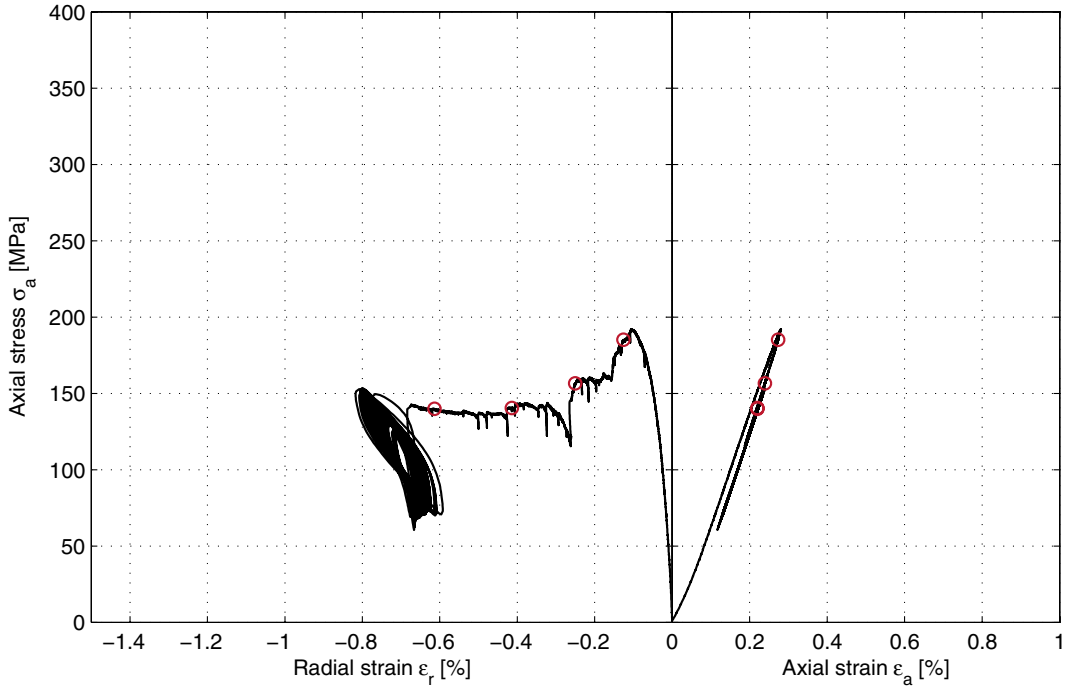

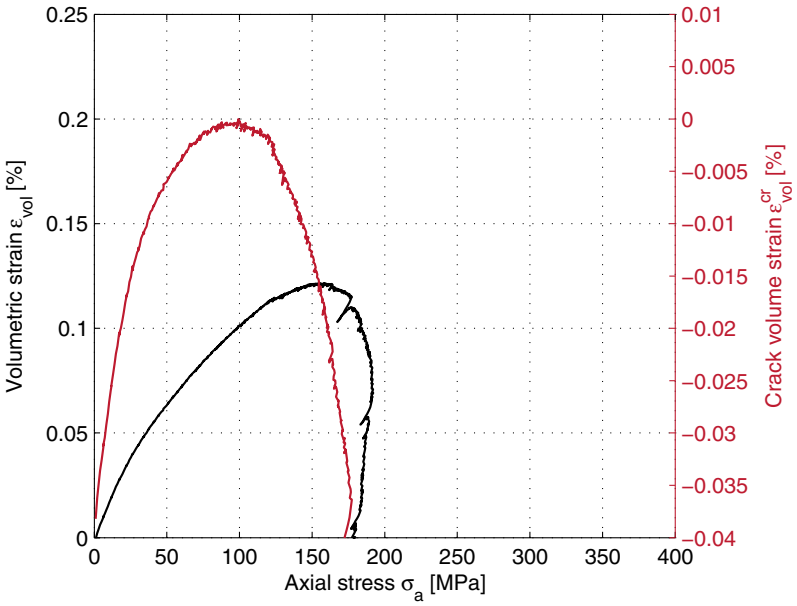

Specimen ID: KFM06A-113-19

Before mechanical test

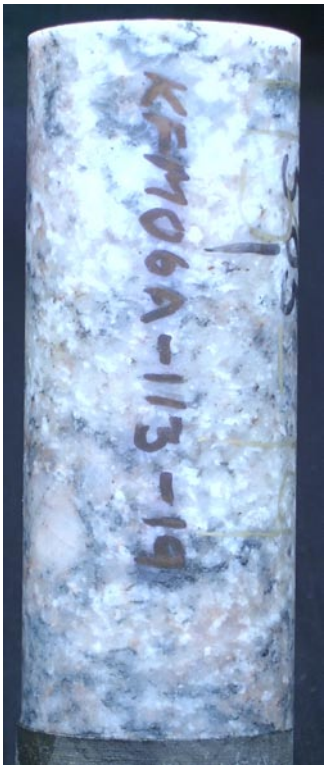

After mechanical test

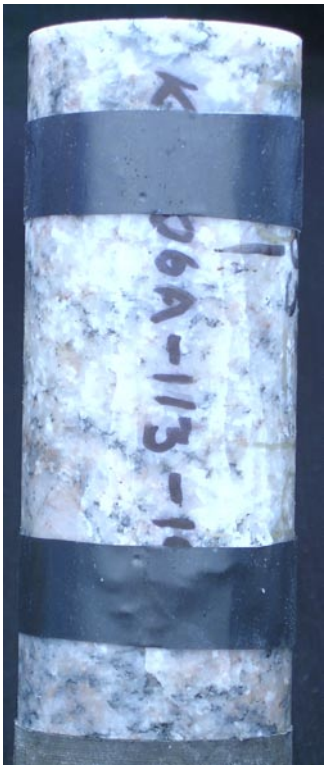

Diameter (mm)	Height (mm)	Density (kg/m^3)
50.7	127.6	2,610

Comments Spalling on one side of the specimen in the longitudinal direction. The load started to oscillate when a crack was formed under the chain whereupon the test was stopped.

Specimen ID: KFM06A−113−19

Youngs Modulus (E):	71.8	[GPa]
Poisson Ratio (ν):	0.345	[−]
Axial peak stress (σ_c):	235.3	[MPa]

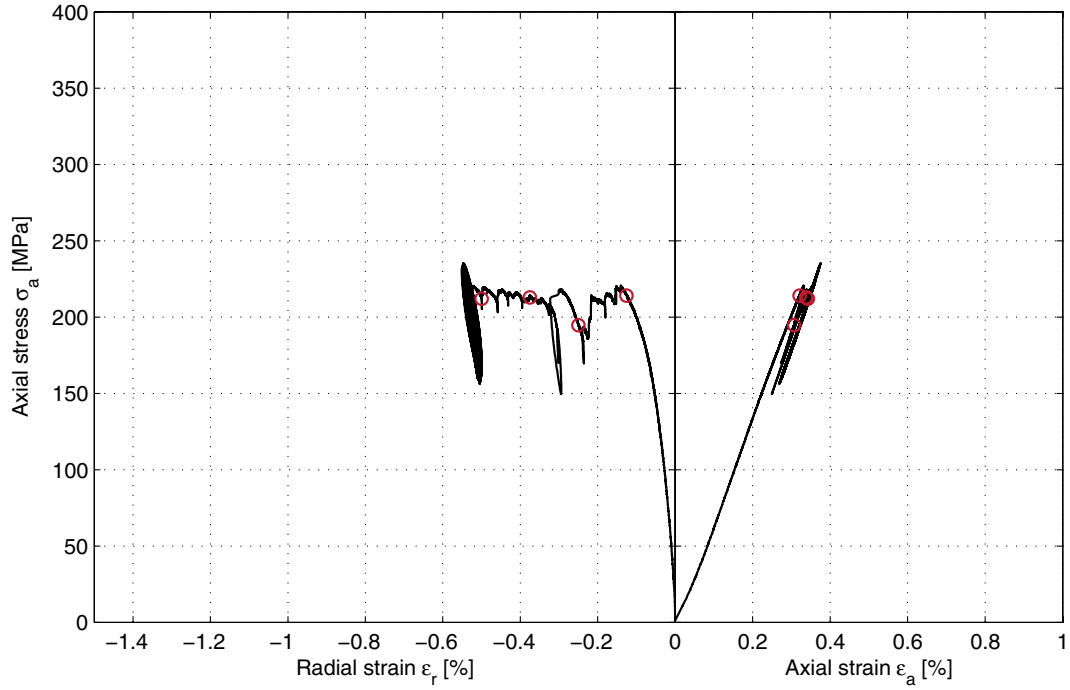

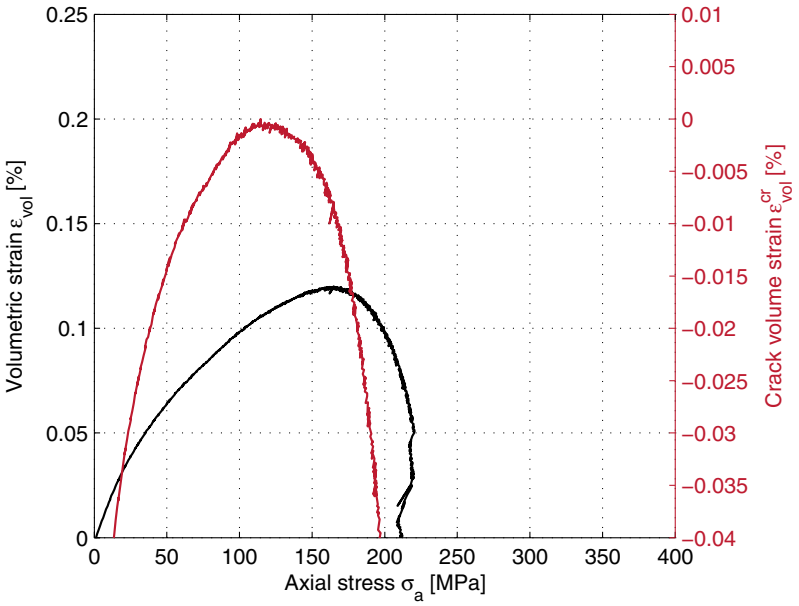

5.2 Results for the entire test series

A summary of the test results is shown in Tables 5-1 and 5-2. The density, uniaxial compressive strength, the tangent Young's modulus and the tangent Poisson ratio versus sampling depth are shown in Figures 5-1 to 5-4.

Table 5-1. Summary of results.

Identification	Density (kg/m³)	Compressive strength (MPa)	Young's modulus (GPa)	Poisson ratio (–)	K_{system} (GN/m)	Rock type
KFM06A-113-1	2,660	214.4	74.7	0.25	6.73	Granite
KFM06A-113-2	2,670	157.0	76.1	0.23	6.39	Granite
KFM06A-113-3	2,670	(126.4)*	76.7	0.19	5.41	Granite
KFM06A-113-4	2,670	180.8	74.3	0.26	6.65	Granite
KFM06A-113-5	2,660	194.8	71.5	0.30	7.05	Granite
KFM06A-113-6	2,670	180.4	70.5	0.29	6.63	Granite
KFM06A-113-9	2,660	229.0	79.6	0.25	5.91	Aplite
KFM06A-113-10	2,650	371.1	80.8	0.31	7.46	Aplite
KFM06A-113-11	2,650	309.1	85.6	0.28	5.25	Aplite
KFM06A-113-12	2,660	357.7	81.7	0.26	6.03	Aplite
KFM06A-113-13	2,660	282.4	85.6	0.25	5.79	Aplite
KFM06A-113-15	2,620	232.0	71.2	0.30	7.66	Pegmatite
KFM06A-113-16	2,630	213.5	72.1	0.27	6.62	Pegmatite
KFM06A-113-17	2,640	235.6	79.8	0.30	5.63	Pegmatite
KFM06A-113-18	2,640	192.1	75.1	0.26	6.04	Pegmatite
KFM06A-113-19	2,610	235.3	71.8	0.35	6.62	Pegmatite

* The value does not represent the strength of a homogenous material.

Table 5-2. Calculated mean values and standard deviation (Std dev) of the results. The value in the parenthesis in Table 5-1 is excluded in calculations of the mean value and the standard deviation.

	Density (kg/m³)	Compressive strength (MPa)	Young's modulus (GPa)	Poisson ratio (–)
Mean value (395–450 m)	2,667	175.6	74.0	0.25
Mean value (483–503 m)	2,628	221.7	74.0	0.29
Mean value (818–820 m)	2,656	309.9	82.7	0.27
Mean value (All levels)	2,651	232.0	76.7	0.27
Std dev (395–450 m)	5.2	30.6	2.5	0.04
Std dev (483–503 m)	13.0	18.9	3.6	0.03
Std dev (818–820 m)	5.5	57.8	2.8	0.02
Std dev (All levels)	18.6	68.0	5.0	0.04

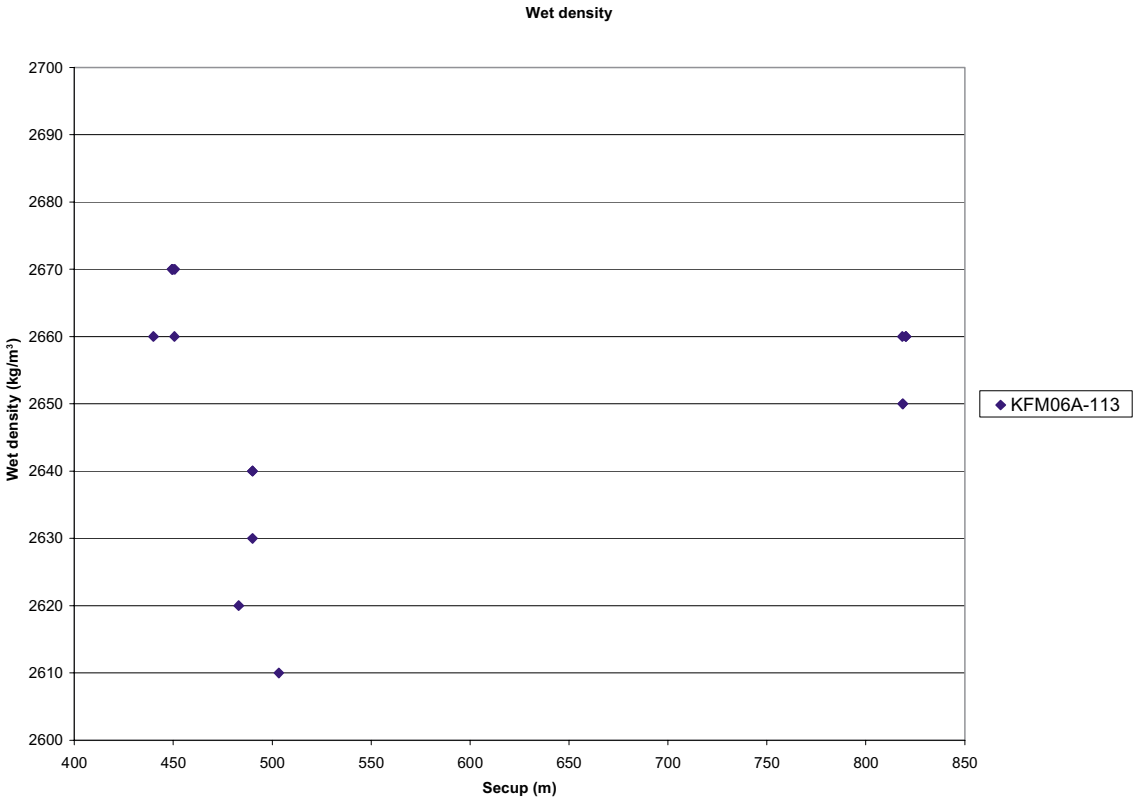

Figure 5-1. *Density versus borehole length (KFM06A is inclined c 60° from the horizon).*

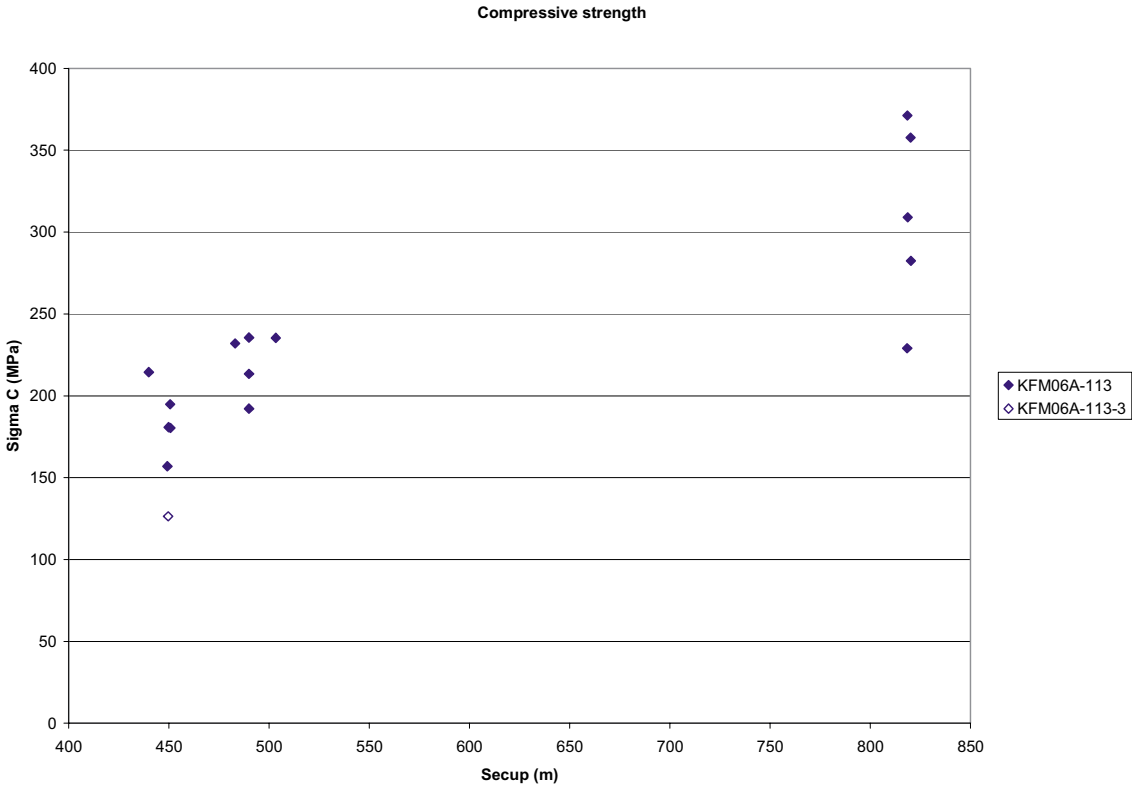

Figure 5-2. *Uniaxial compressive strength versus borehole length (KFM06A is inclined c 60° from the horizon).*

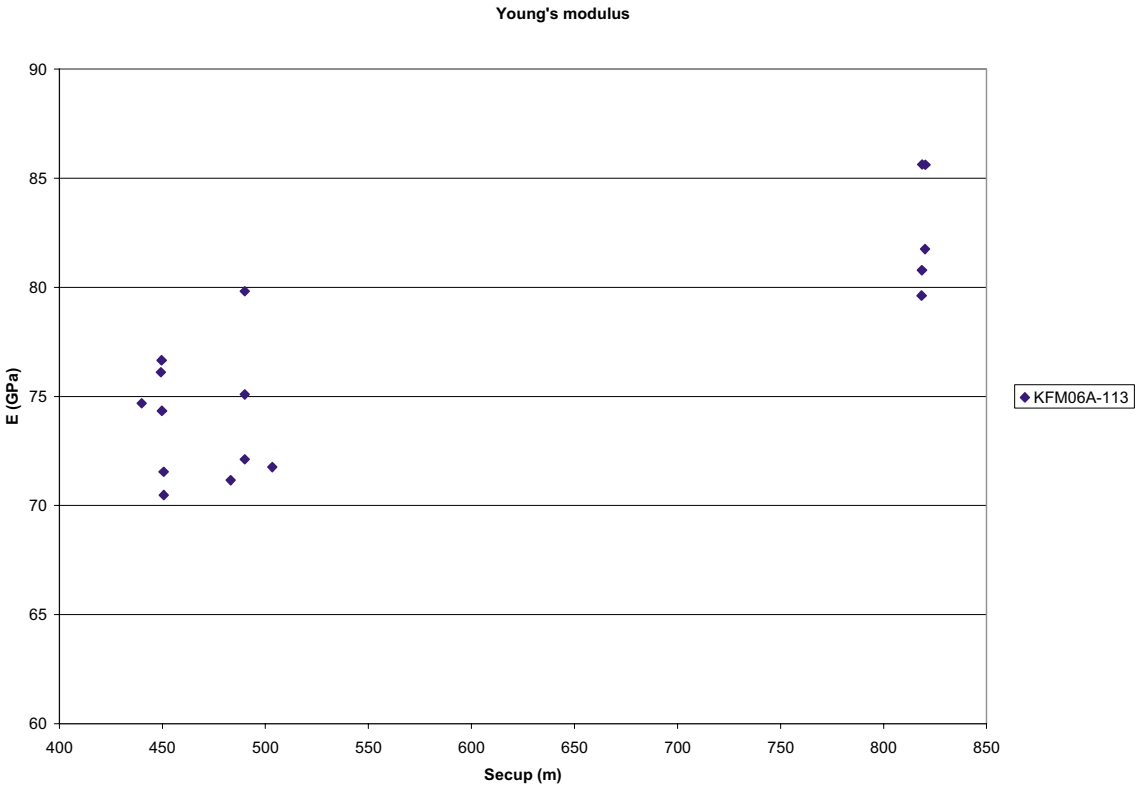

Figure 5-3. *Tangent Young's modulus versus borehole length (KFM06A is inclined c 60° from the horizon).*

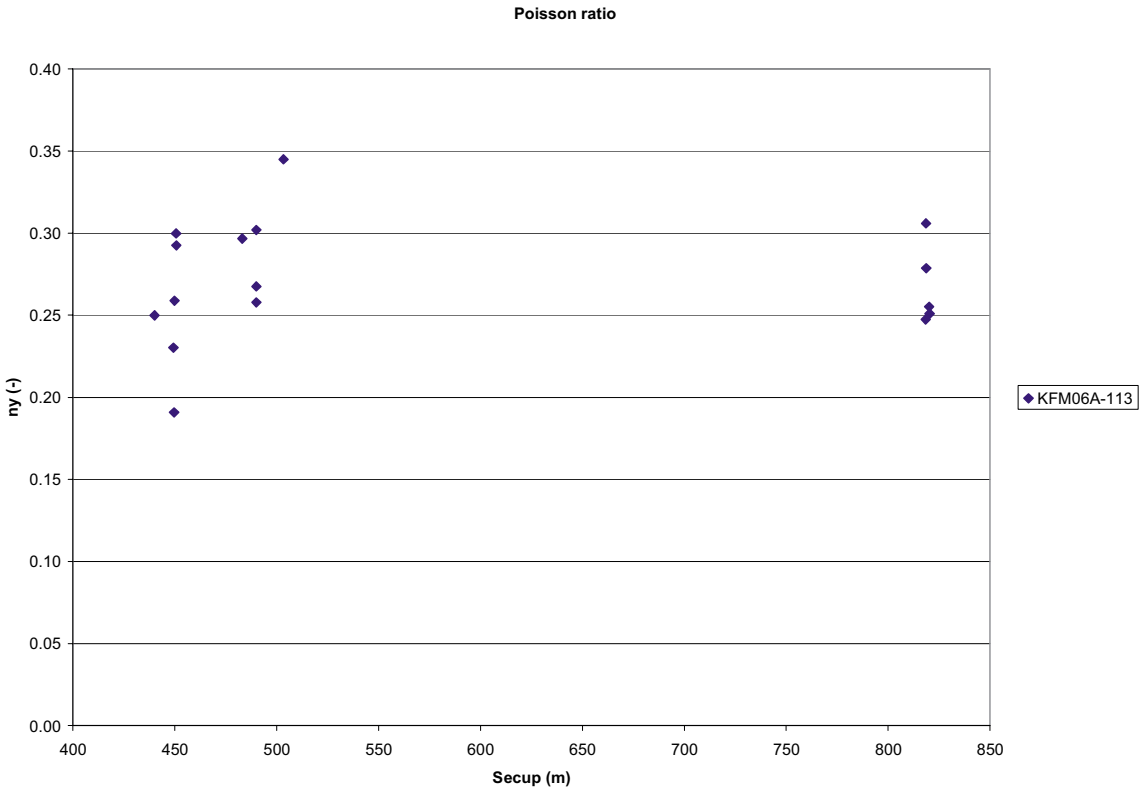

Figure 5-4. *Tangent Poisson ratio versus borehole length (KFM06A is inclined c 60° from the horizon).*

5.3 Discussion

The core was slightly curved in the area of the 450 m depth level. Hence, the specimens KFM06A-113-1 to KFM06A-113-6 had a certain curvature. The deviation from a completely straight specimen was between 0.15–0.25 mm. However, this is within the valid range of the specified geometry tolerances as stated in /1/.

The tested specimens have a rock structure with foliations of varying degree which clearly has affected the failure in some cases. Examples of the rock structure from the three different depth levels are shown in Figure 5-5. The crack development in one of the end surfaces can be seen in the left picture in Figure 5-5. Furthermore, it should be expected that the specimens have an anisotropic response in general.

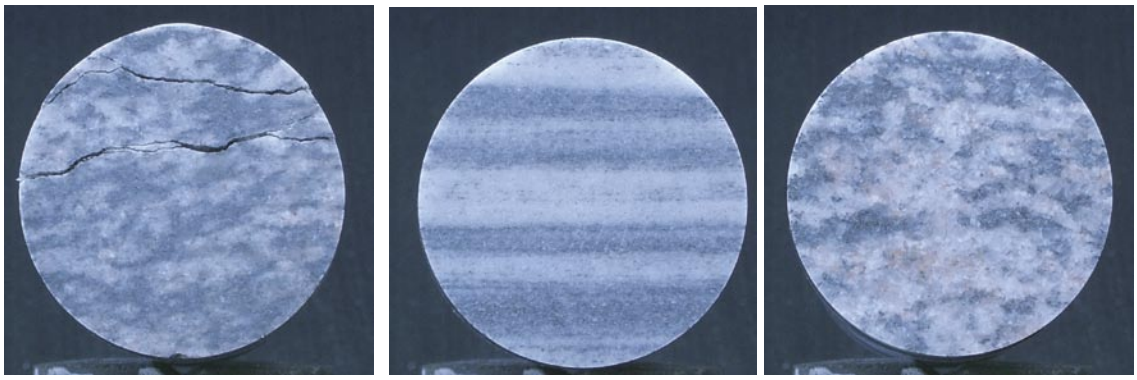

Figure 5-5. *The end surfaces of specimens KFM06A-113-2 (left), KFM06A-113-9 (middle) and KFM06A-113-16 (right).*

References

/1/ **ISRM, 1999.** Draft ISRM suggested method for the complete stress-strain curve for intact rock in uniaxial compression. Int. J. Rock. Mech. Min. Sci. 36(3), pp 279–289.

/2/ **Martin C D, Chandler N A, 1994.** The progressive fracture of Luc du Bonnet granite. Int. J. Rock. Mech. Min. Sci. & Geomech. Abstr. 31(6), pp 643–659.

/3/ **Eberhardt E, Stead D, Stimpson B, Read R S, 1998.** Identifying crack initiation and propagation thresholds in brittle rock. Can. Geotech. J. 35, pp 222–233.

/4/ **ASTM 4543-01, 2001.** Standard practice for preparing rock core specimens and determining dimensional and shape tolerance.

/5/ **ISRM, 1979.** Suggested Method for Determining Water Content, Porosity, Density, Absorption and Related Properties and Swelling and Slake-durability Index Properties. Int. J. Rock. Mech. Min. Sci. & Geomech. Abstr. 16(2), pp 141–156.

/6/ **SS-EN 13755.** Natural stone test methods – Determination of water absorption at atmospheric pressure.

/7/ **Stråhle A, 2001.** Definition och beskrivning av parametrar för geologisk, geofysisk och bergmekanisk kartering av berg. SKB R-01-19. Svensk Kärnbränslehantering AB. In Swedish.

/8/ **MATLAB, 2002.** The Language of Technical computing. Version 6.5. MathWorks Inc.

Appendix A

The following equations describe the calculation of radial strains when using a circumferential deformation device, see Figure A-1.

$$\varepsilon_r = \frac{\Delta C}{C_i}$$

where

C_i = $2\,\pi\,R_i$ = initial specimen circumference

ΔC = change in specimen circumference = $\dfrac{\pi \cdot \Delta X}{\sin\left(\dfrac{\theta_i}{2}\right) + \left(\pi - \dfrac{\theta_i}{2}\right)\cos\left(\dfrac{\theta_i}{2}\right)}$

and

ΔX = change in LVDT reading = $X_i - X_f$ (X_i = initial chain gap; X_f = current chain gap)

θ_i = initial chord angle = $2\,\pi - \dfrac{L_c}{R_i + r}$

L_c = chain length (measured from center of one end roller to center of other end roller)

r = roller radius

R_i = initial specimen radius

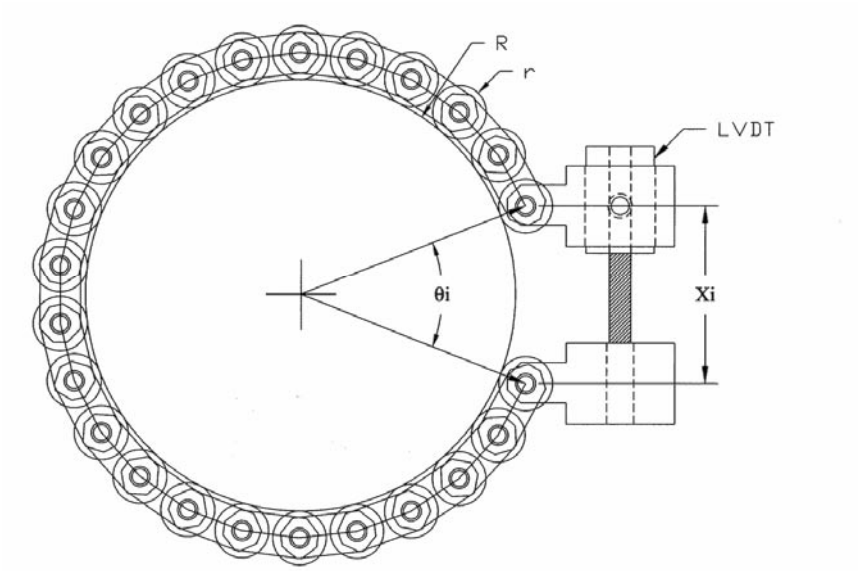

Figure A-1. *Chain for radial deformation measurement.*

Appendix B

This appendix contains results showing the unprocessed data and values on the computed system stiffness K_{system} that was used for the data processing, cf Section 4.4. In addition graphs showing the volumetric strain ε_{vol} versus the axial strain ε_a and the actual radial strain rate $d\varepsilon_r/dt$ versus time are displayed.

Specimen ID: KFM06A−113−01

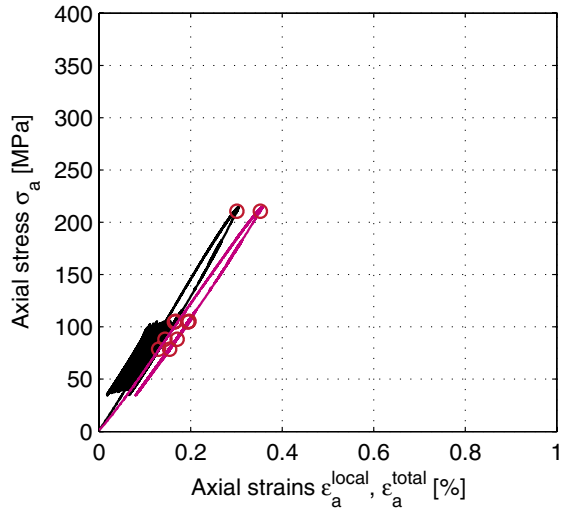

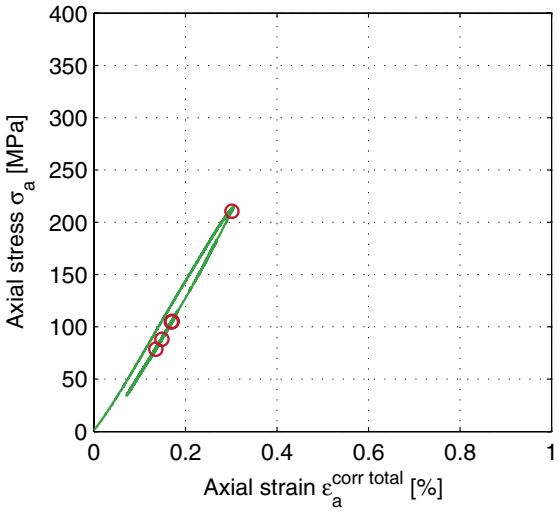

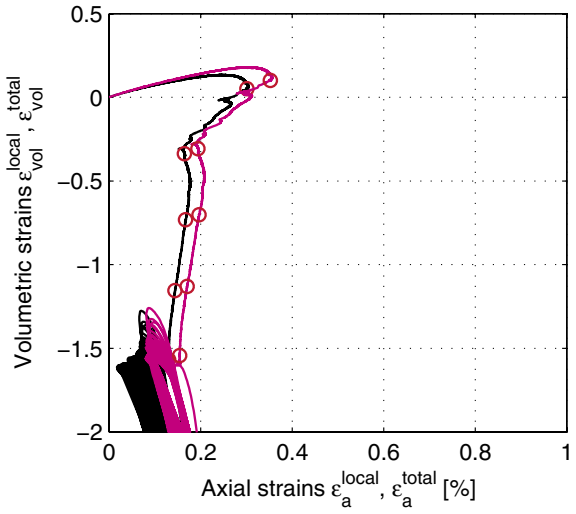

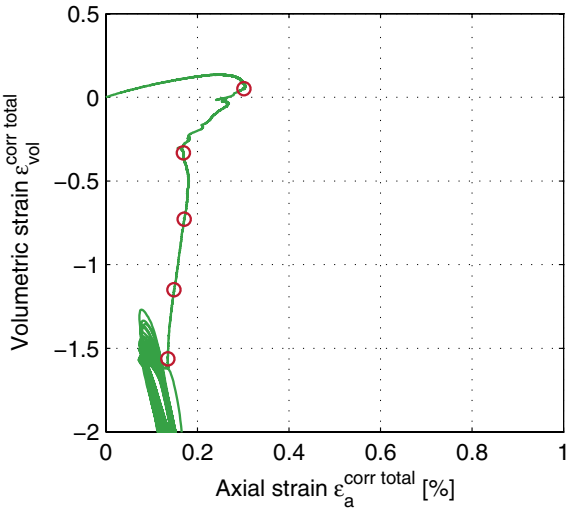

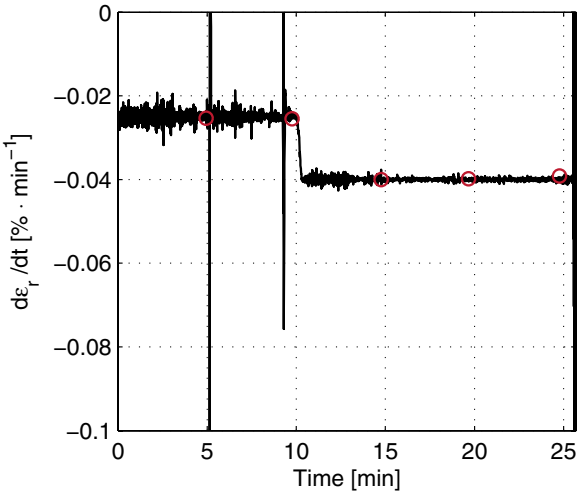

Explanation to curves above:

Based on local deformation (black)

Based on total deformation (magenta)

Based on corrected deformation (green)

Calculated system stiffness:

K_{system} = 6.7276 [GN/m]

Specimen ID: KFM06A−113−02

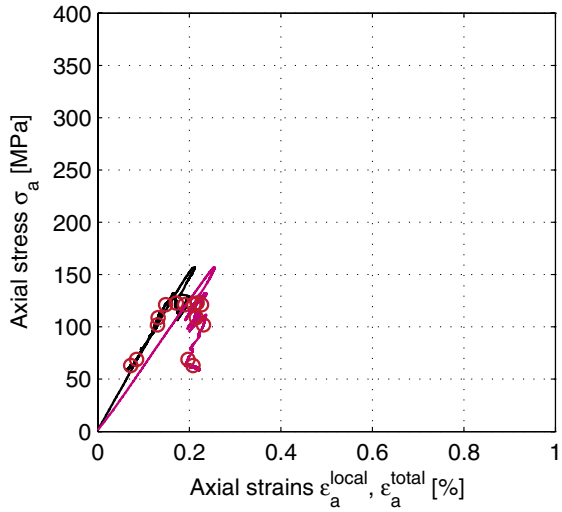

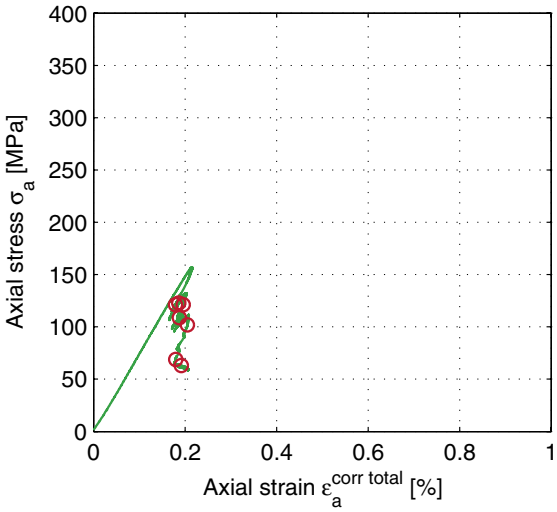

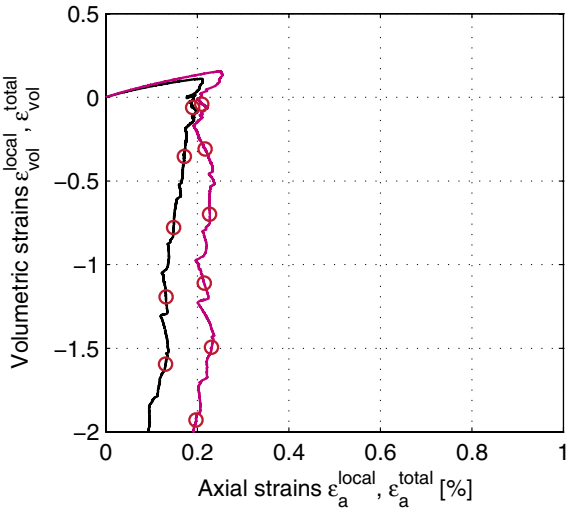

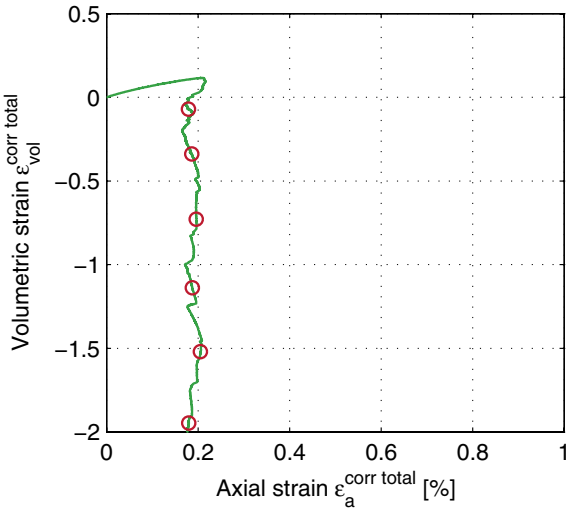

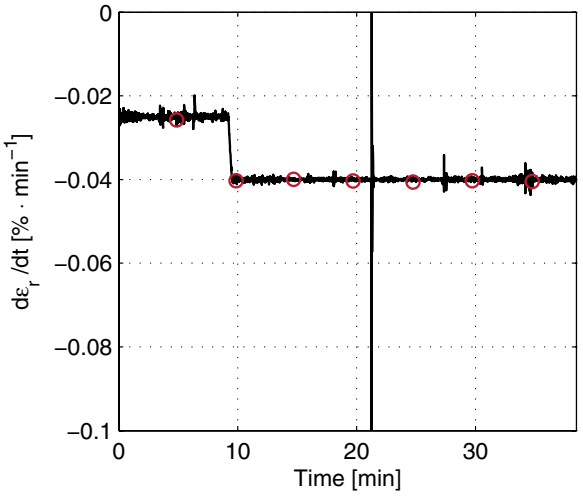

Explanation to curves above:

Based on local deformation (black)

Based on total deformation (magenta)

Based on corrected deformation (green)

Calculated system stiffness:

K_{system} = 6.3932 [GN/m]

Specimen ID: KFM06A−113−03

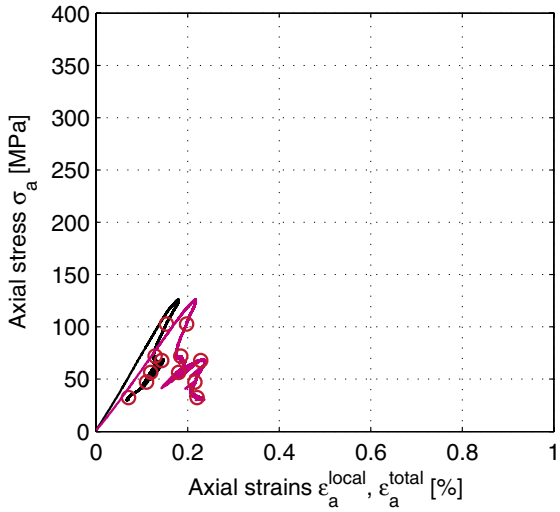

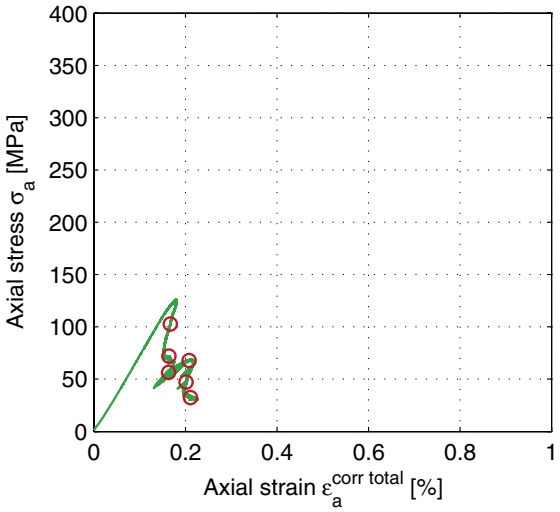

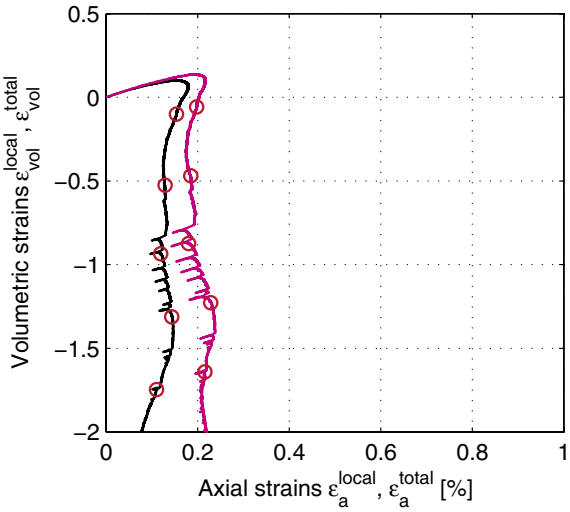

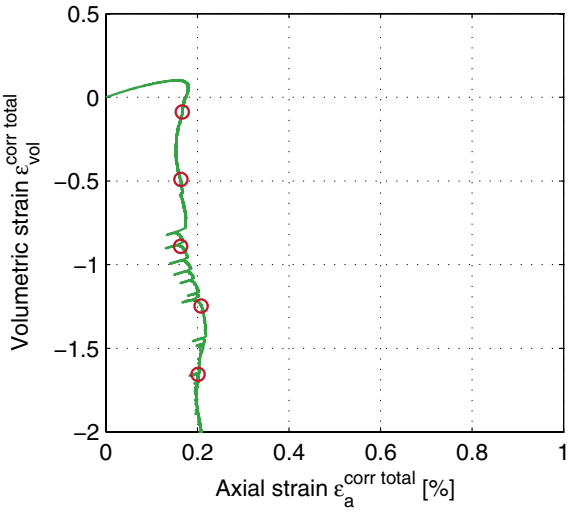

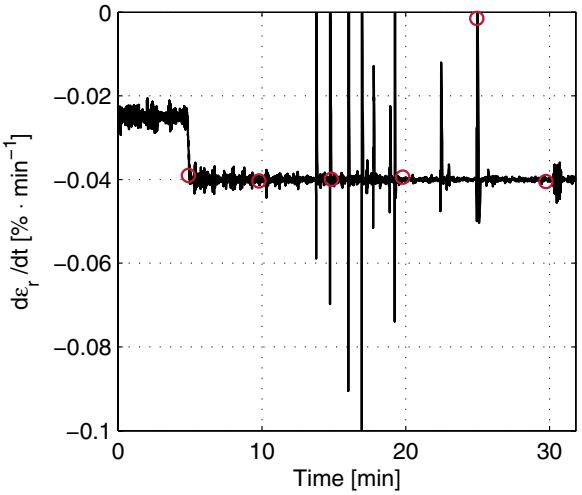

Explanation to curves above:

Based on local deformation (black)

Based on total deformation (magenta)

Based on corrected deformation (green)

Calculated system stiffness:

K_{system} = 5.407 [GN/m]

Specimen ID: KFM06A–113–04

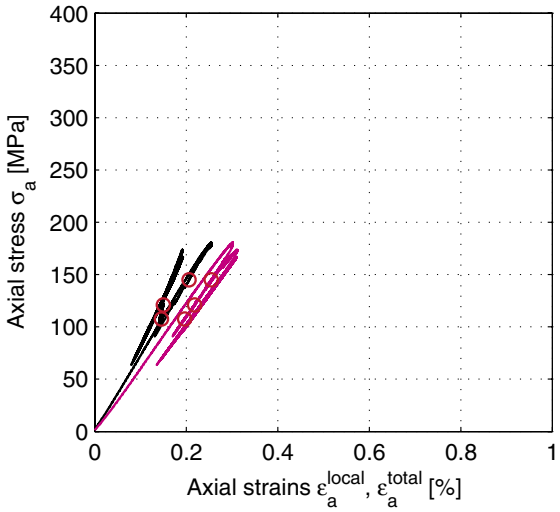

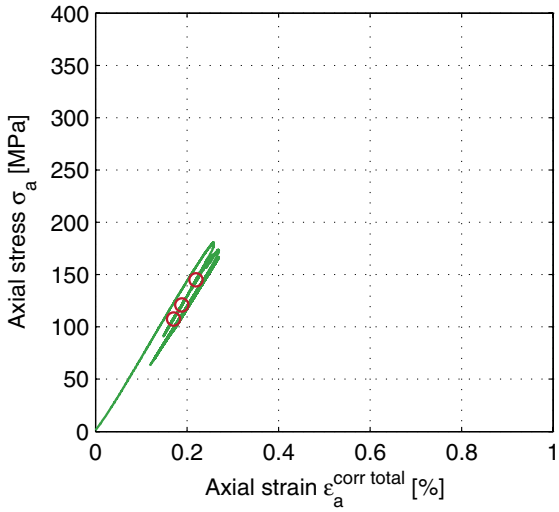

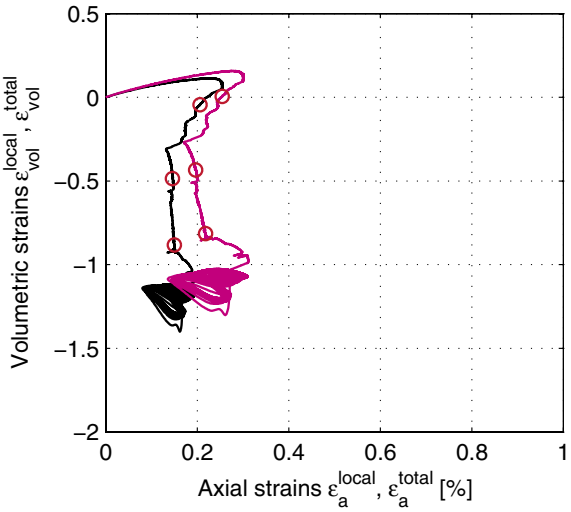

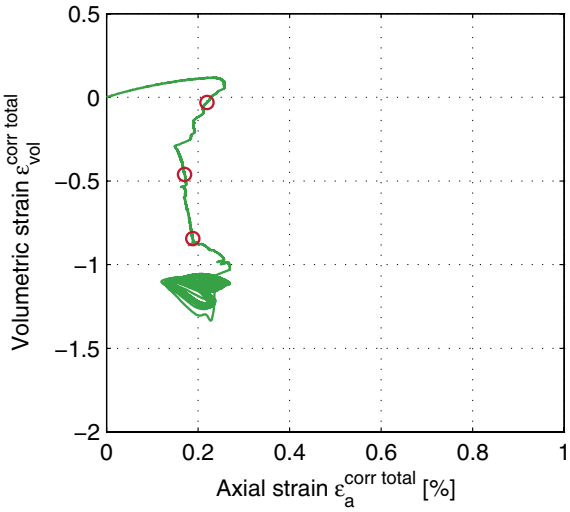

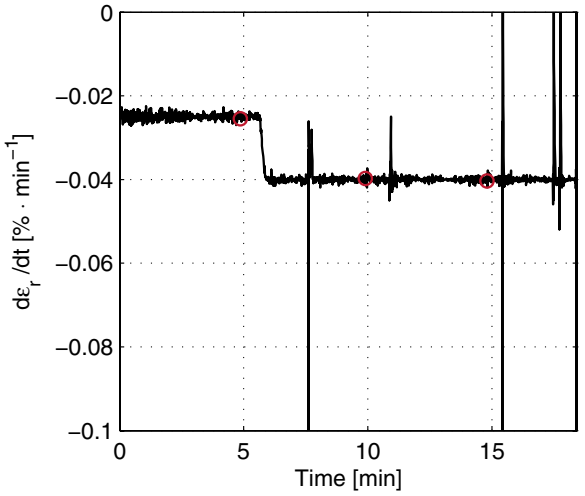

Explanation to curves above:

Based on local deformation (black)

Based on total deformation (magenta)

Based on corrected deformation (green)

Calculated system stiffness:

K_{system} = 6.6513 [GN/m]

Specimen ID: KFM06A–113–05

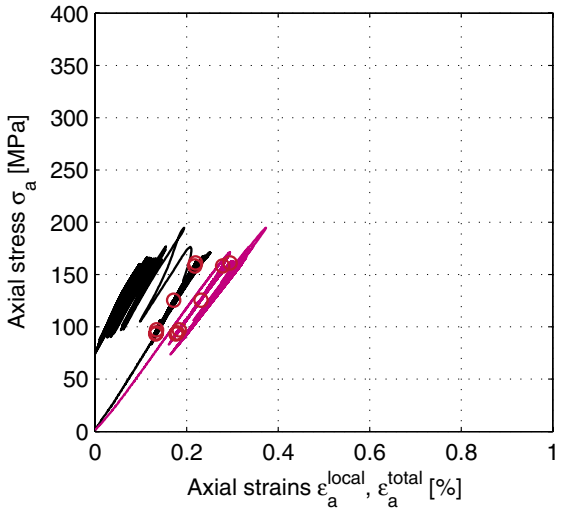

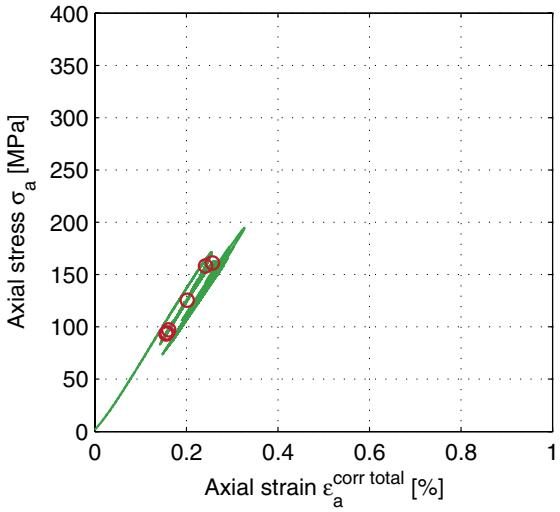

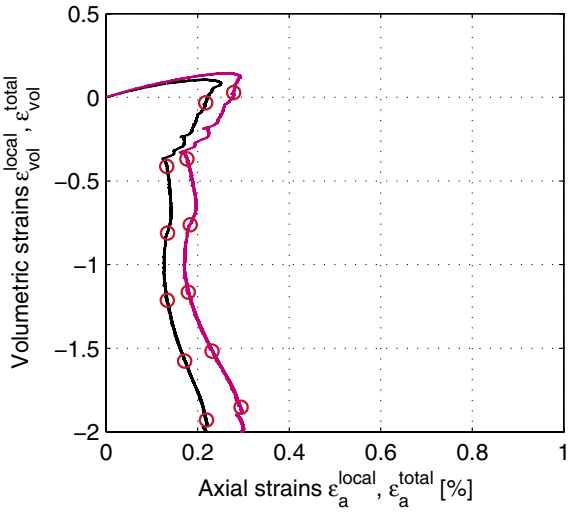

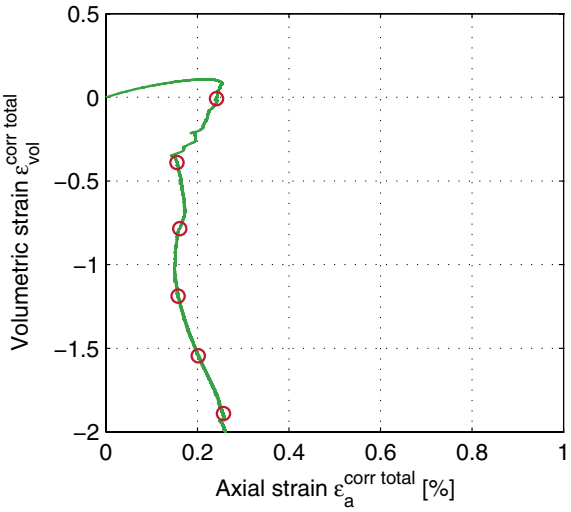

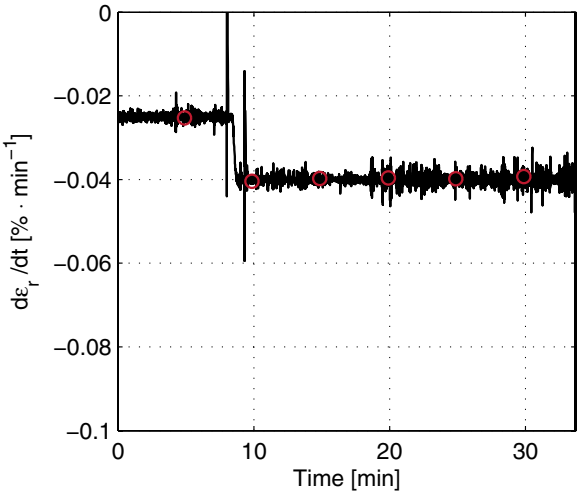

Explanation to curves above:

Based on local deformation (black)

Based on total deformation (magenta)

Based on corrected deformation (green)

Calculated system stiffness:

K_{system} = 7.0548 [GN/m]

Specimen ID: KFM06A−113−06

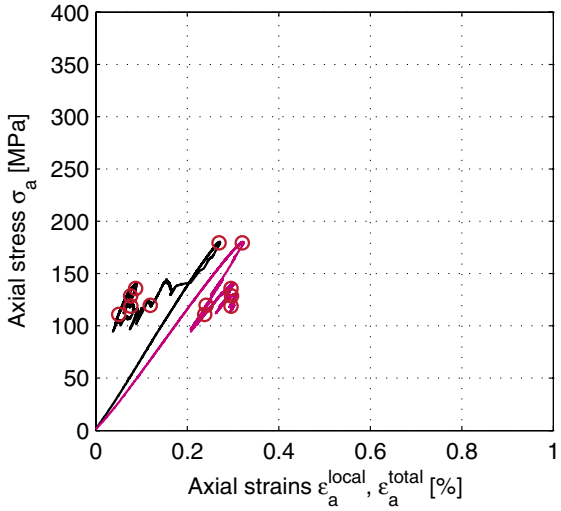

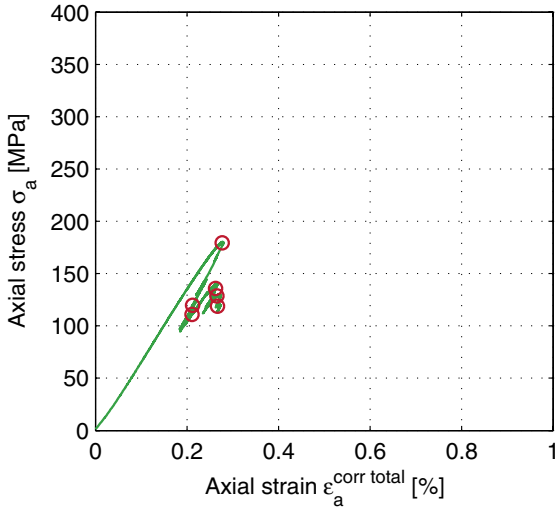

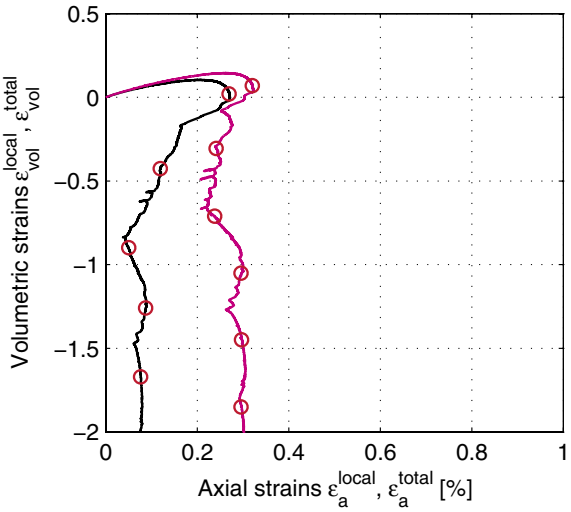

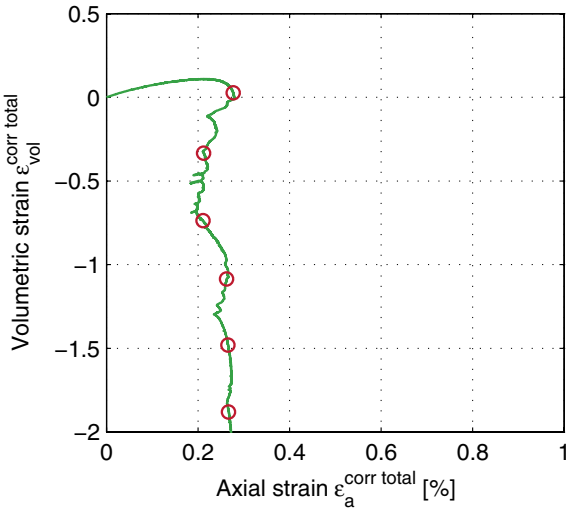

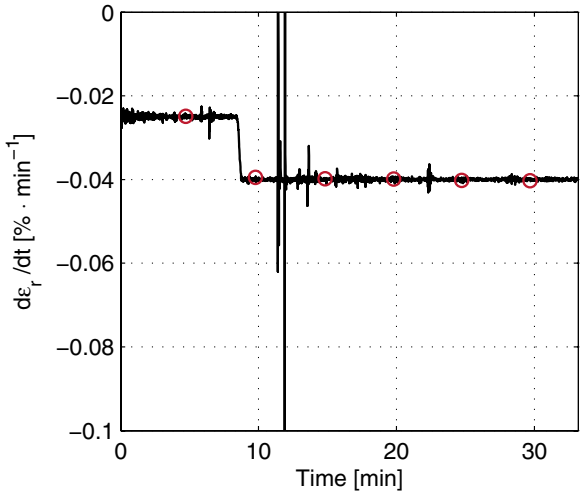

Explanation to curves above:

Based on local deformation (black)

Based on total deformation (magenta)

Based on corrected deformation (green)

Calculated system stiffness:

K_{system} = 6.6251 [GN/m]

Specimen ID: KFM06A−113−09

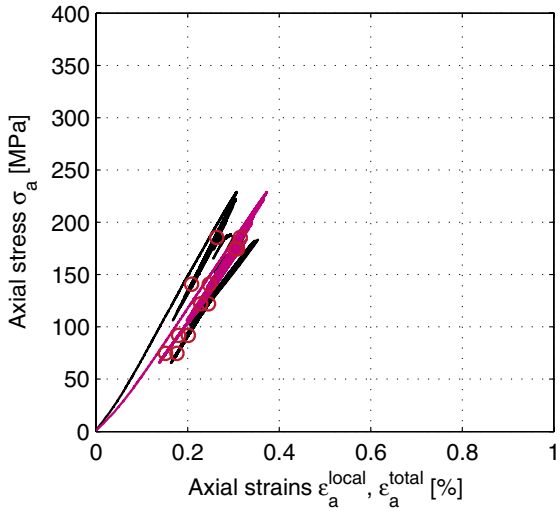

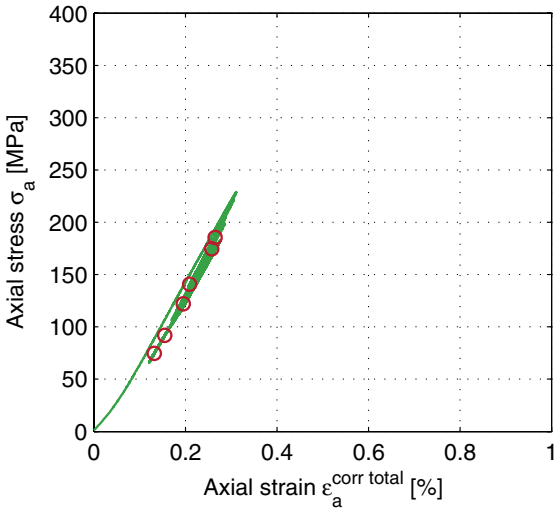

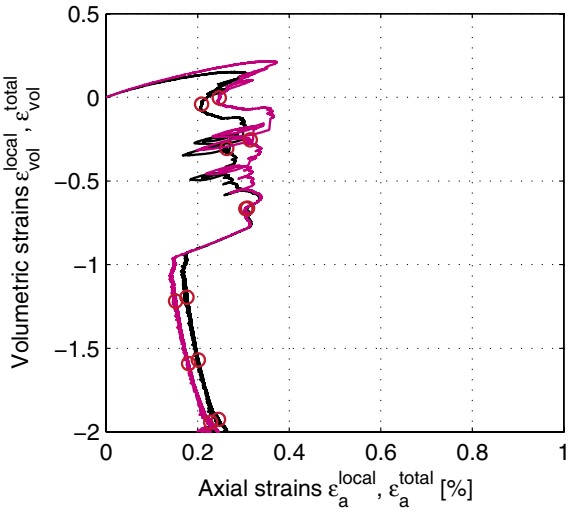

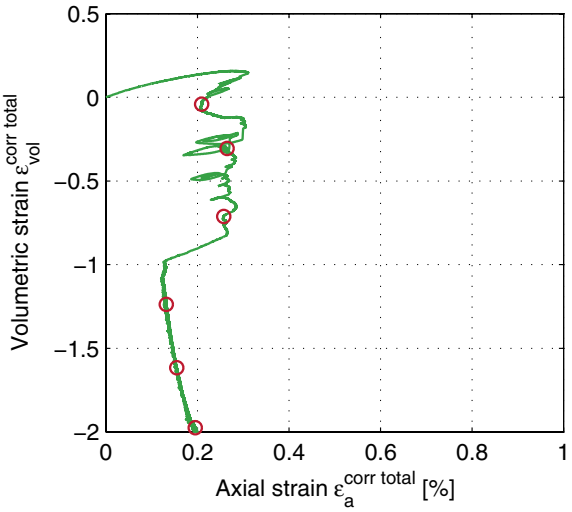

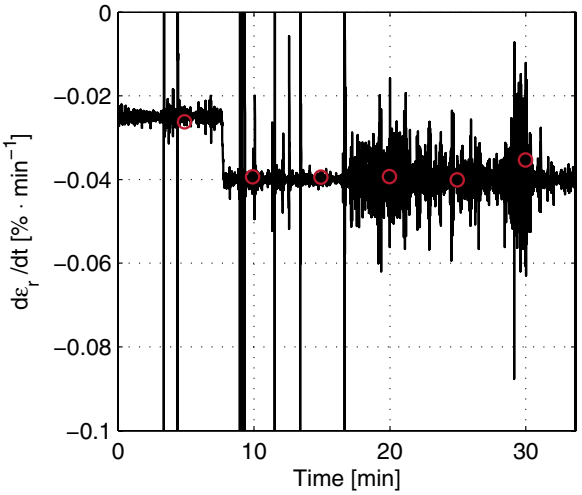

Explanation to curves above:

Based on local deformation (black)

Based on total deformation (magenta)

Based on corrected deformation (green)

Calculated system stiffness:

K_{system} = 5.9065 [GN/m]

Specimen ID: KFM06A–113–10

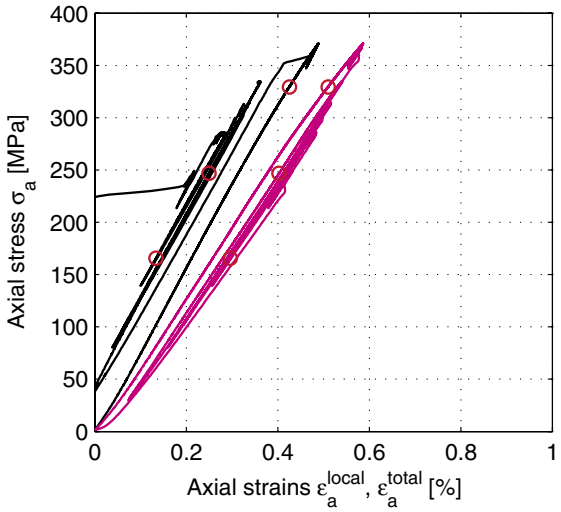

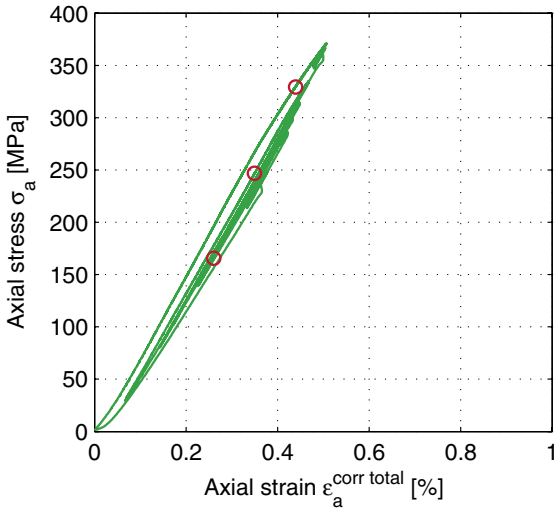

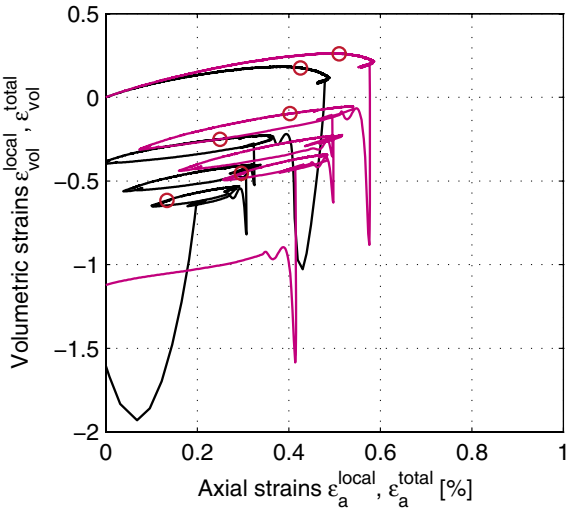

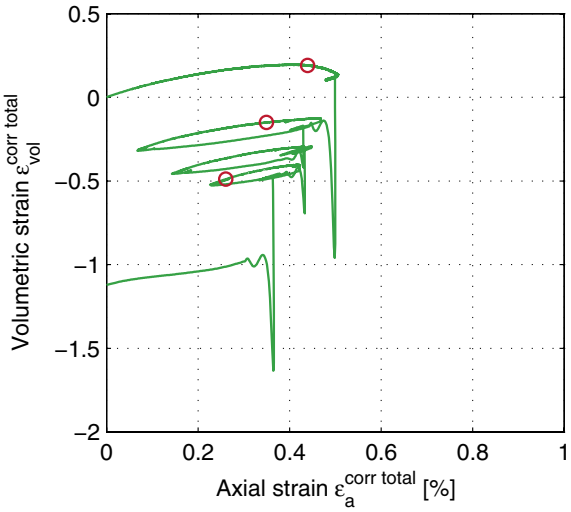

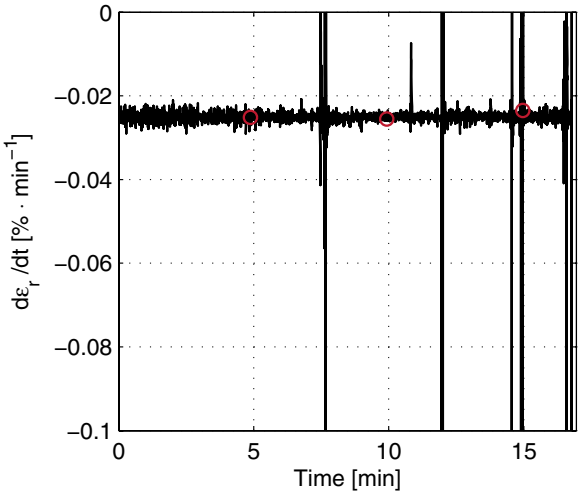

Explanation to curves above:

Based on local deformation (black)

Based on total deformation (magenta)

Based on corrected deformation (green)

Calculated system stiffness:

K_{system} = 7.4569 [GN/m]

Specimen ID: KFM06A–113–11

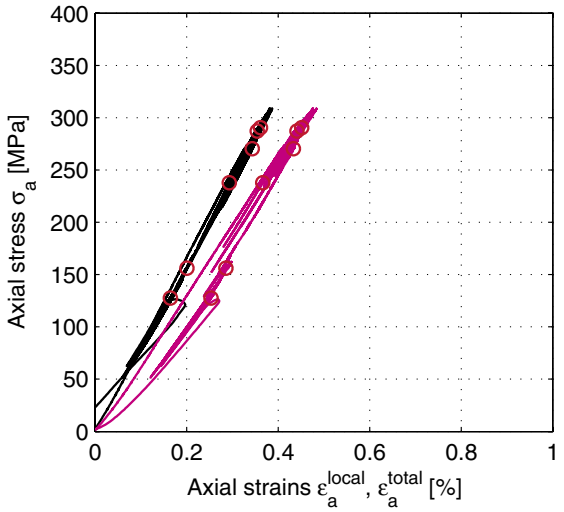

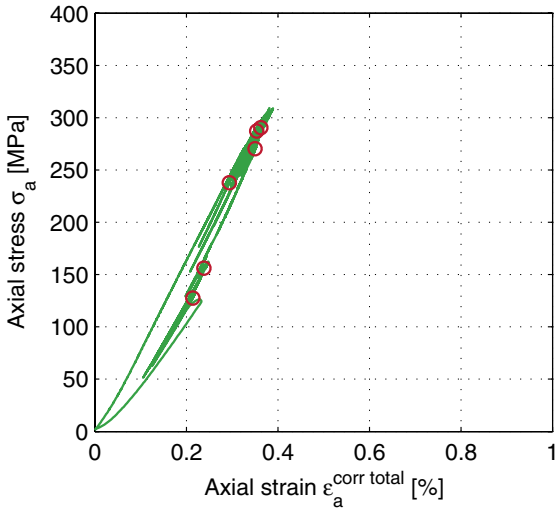

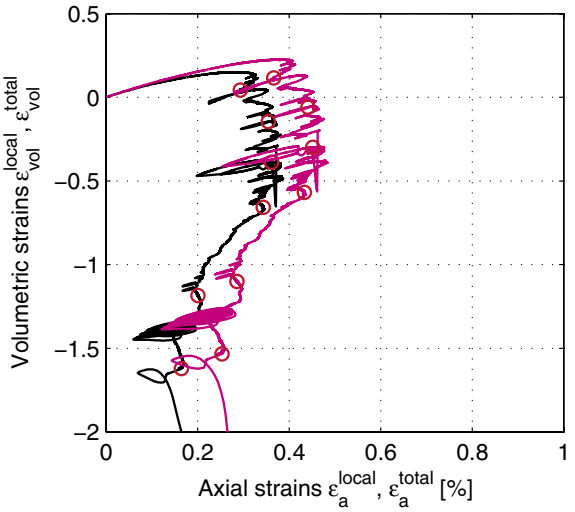

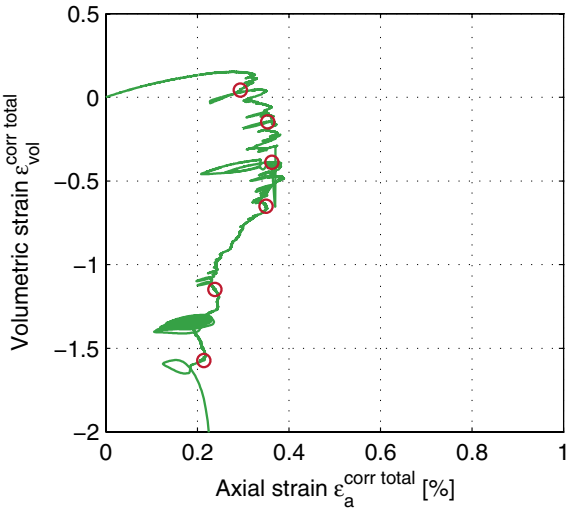

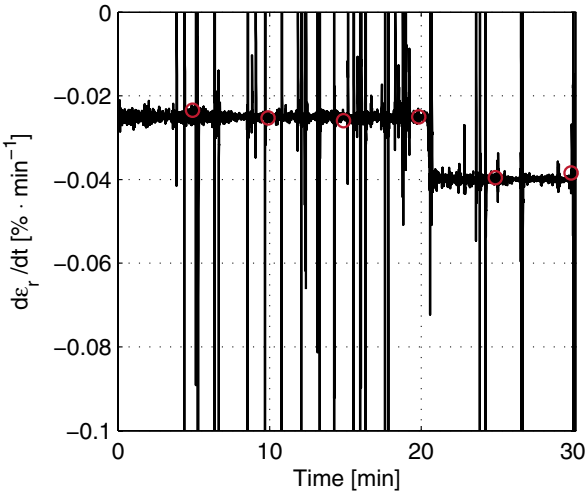

Explanation to curves above:

Based on local deformation (black)

Based on total deformation (magenta)

Based on corrected deformation (green)

Calculated system stiffness:

K_{system} = 5.2489 [GN/m]

Specimen ID: KFM06A–113–12

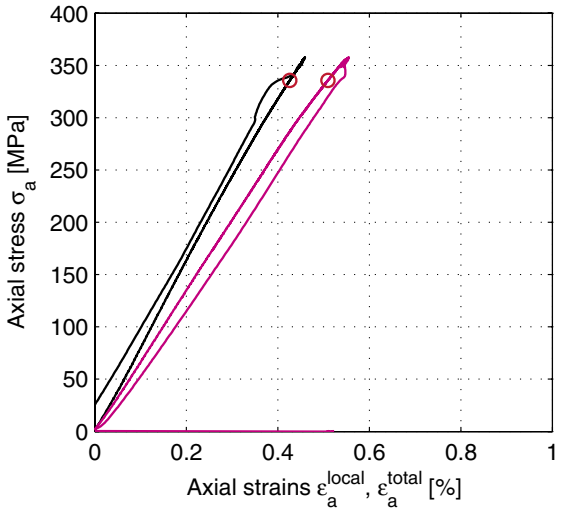

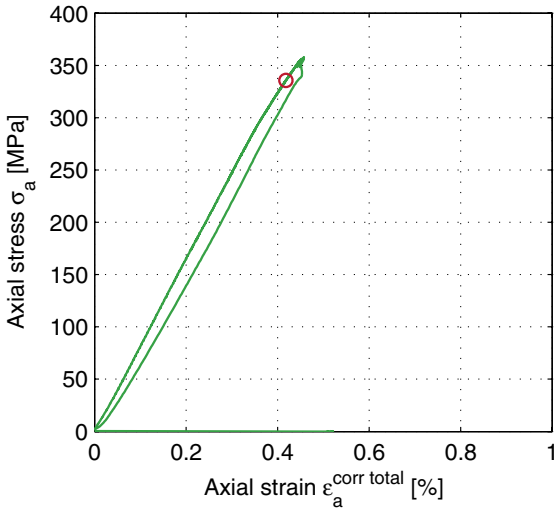

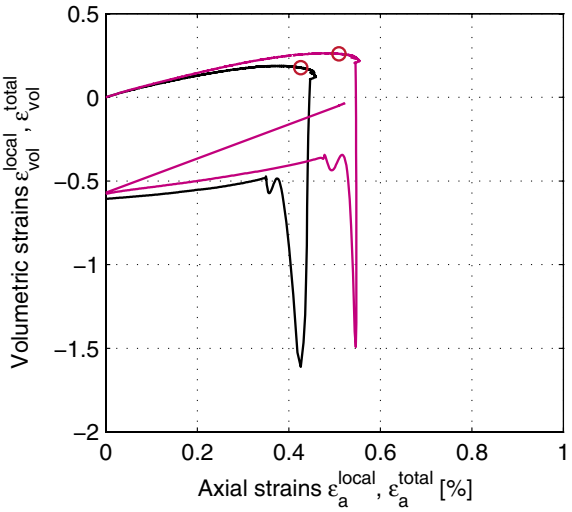

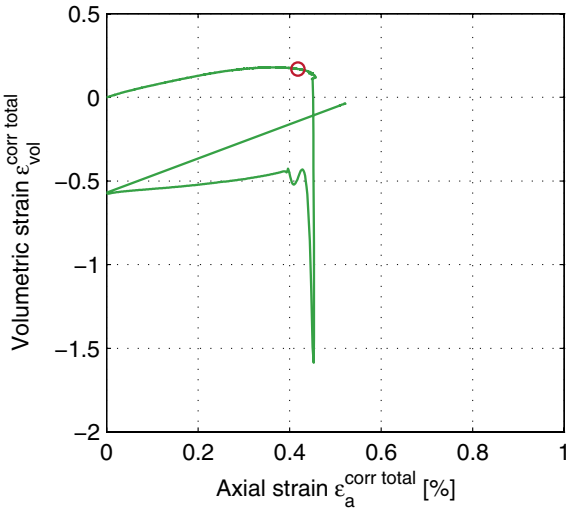

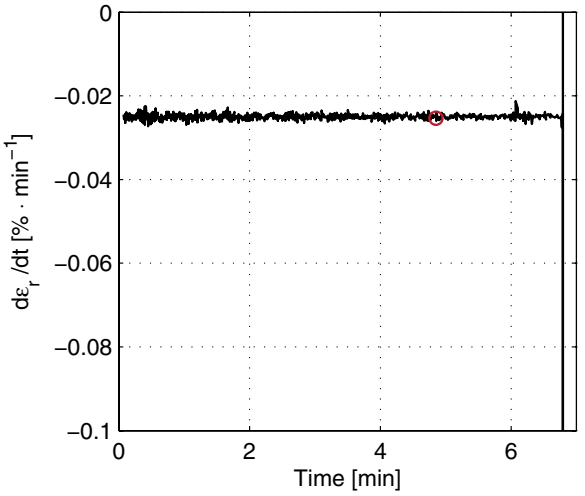

Explanation to curves above:

Based on local deformation (black)

Based on total deformation (magenta)

Based on corrected deformation (green)

Calculated system stiffness:

K_{system} = 6.0306 [GN/m]

Specimen ID: KFM06A–113–13

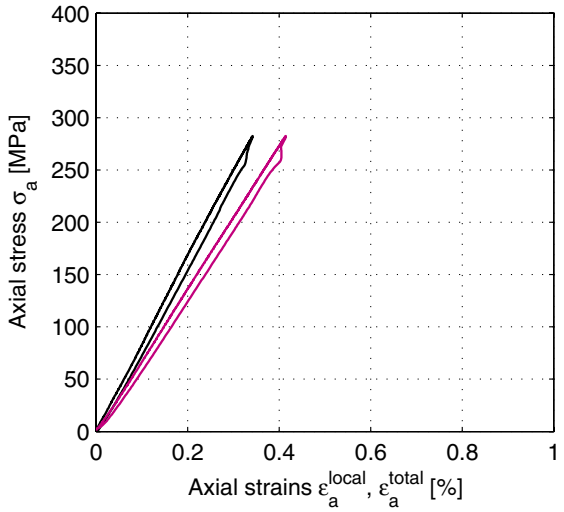

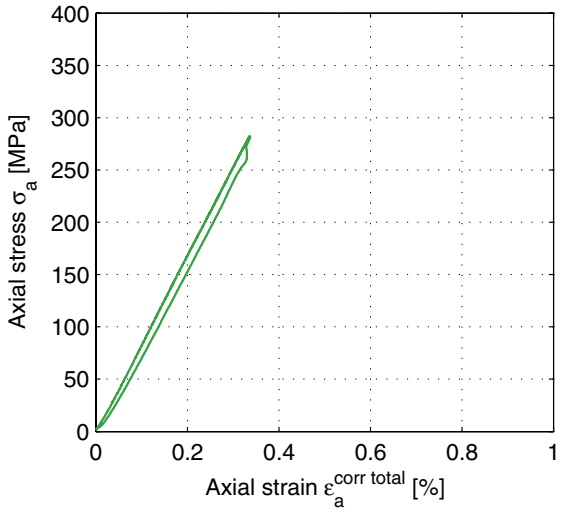

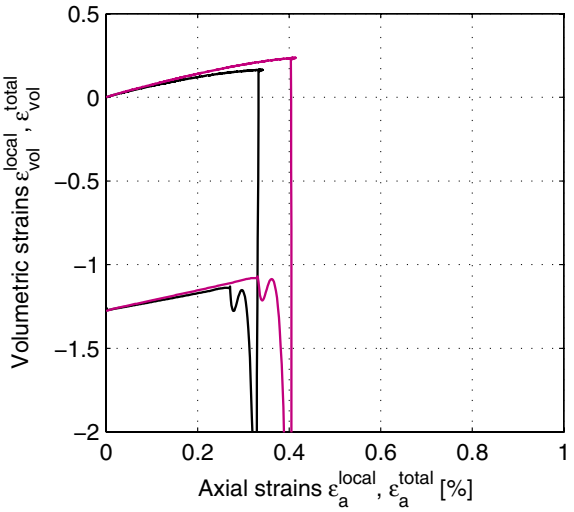

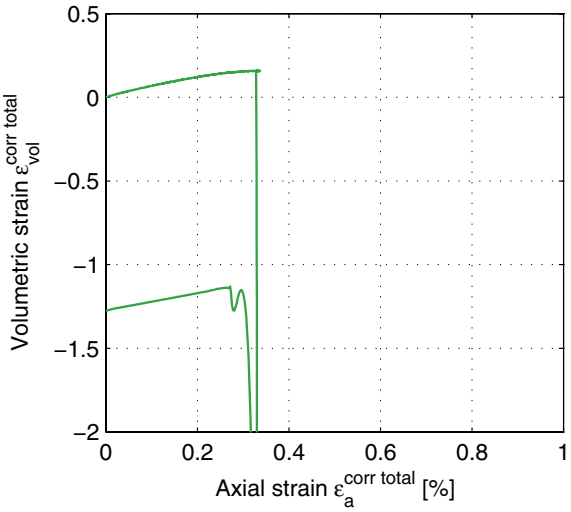

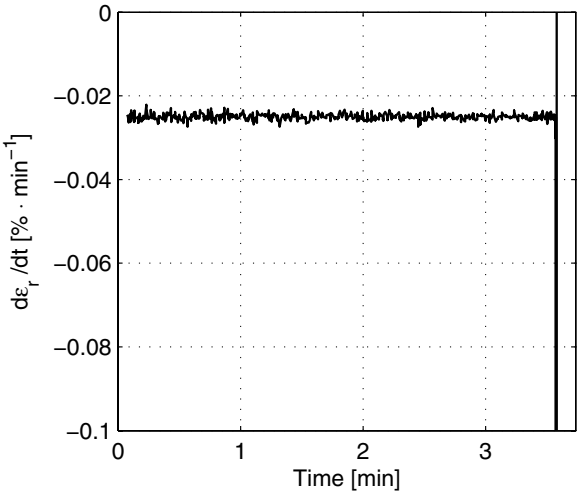

Explanation to curves above:

Based on local deformation (black)

Based on total deformation (magenta)

Based on corrected deformation (green)

Calculated system stiffness:

K_{system} = 5.7916 [GN/m]

Specimen ID: KFM06A–113–15

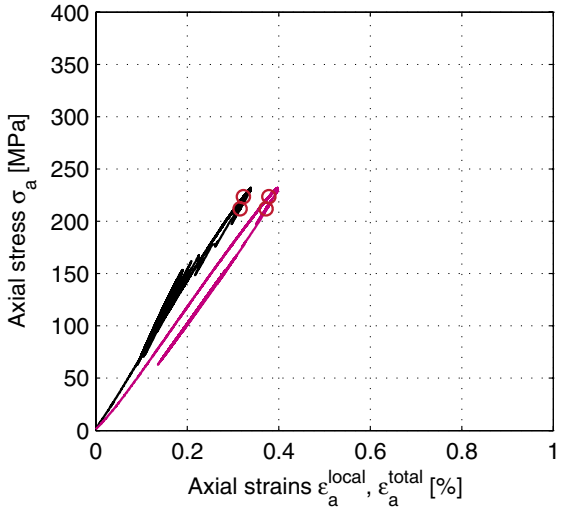

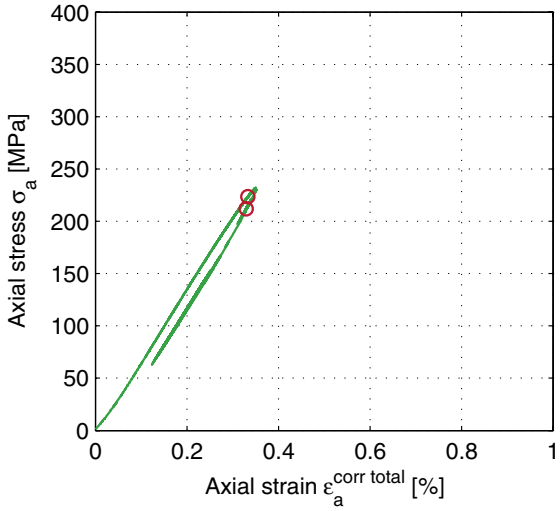

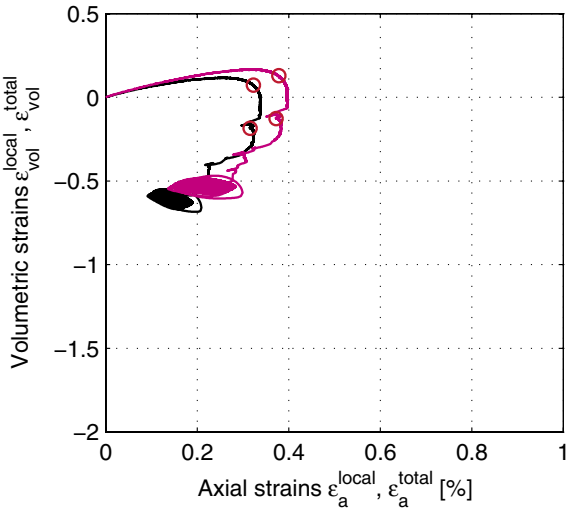

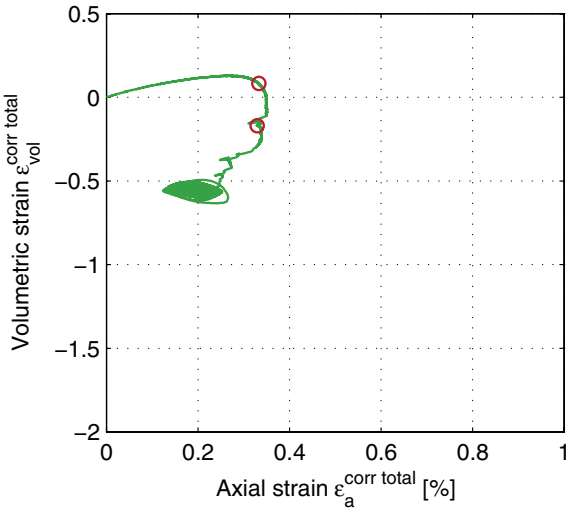

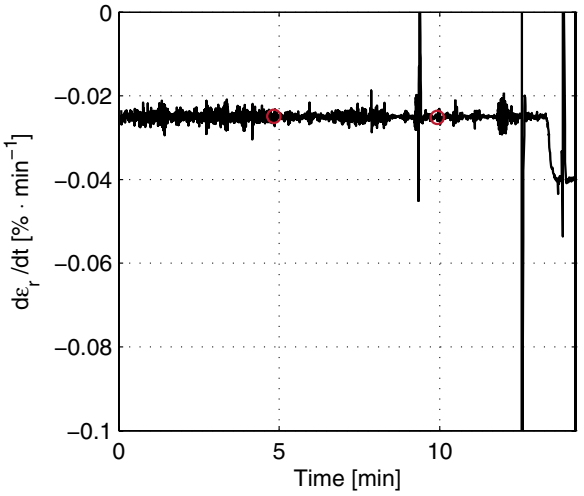

Explanation to curves above:

Based on local deformation (black)

Based on total deformation (magenta)

Based on corrected deformation (green)

Calculated system stiffness:

K_{system} = 7.6608 [GN/m]

Specimen ID: KFM06A–113–16

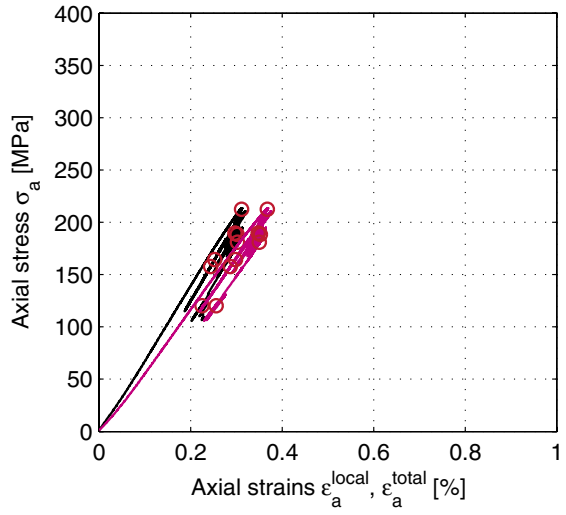

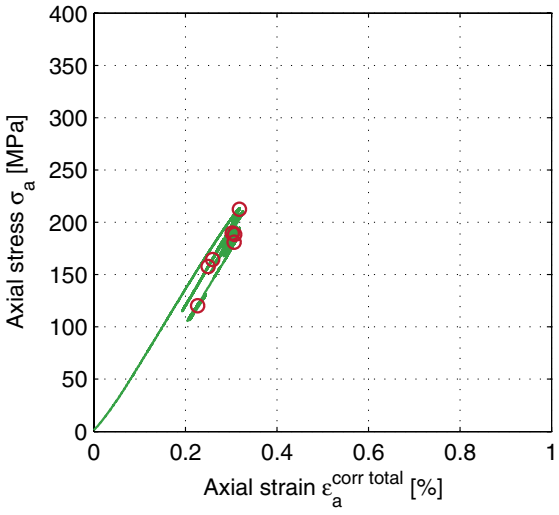

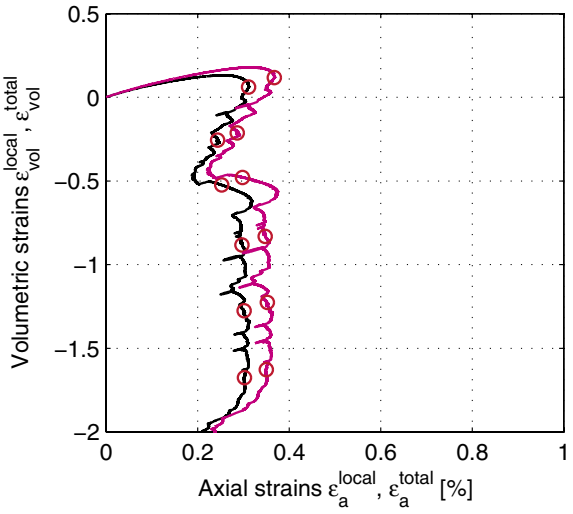

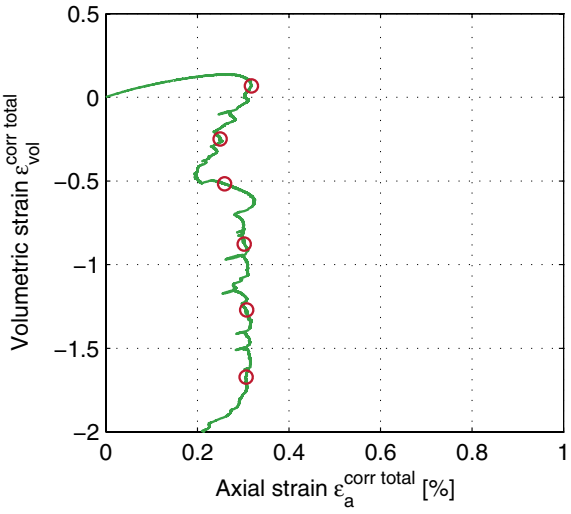

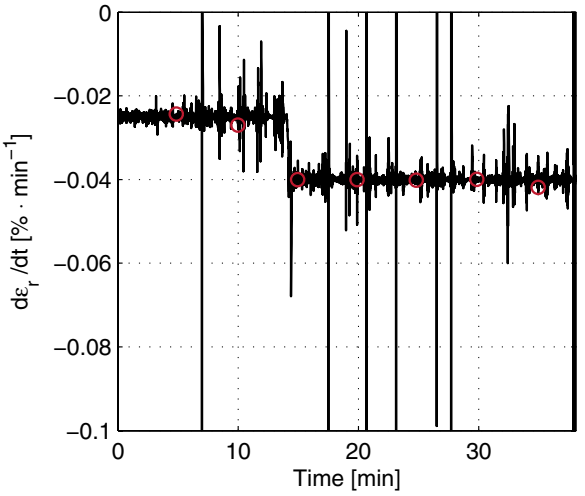

Explanation to curves above:

Based on local deformation (black)

Based on total deformation (magenta)

Based on corrected deformation (green)

Calculated system stiffness:

K_{system} = 6.6237 [GN/m]

Specimen ID: KFM06A−113−17

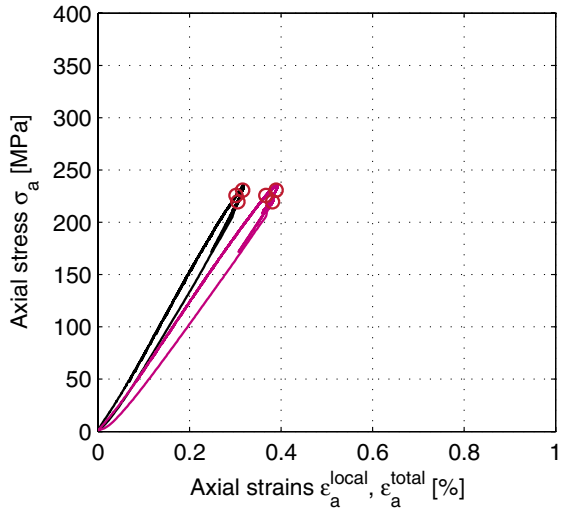

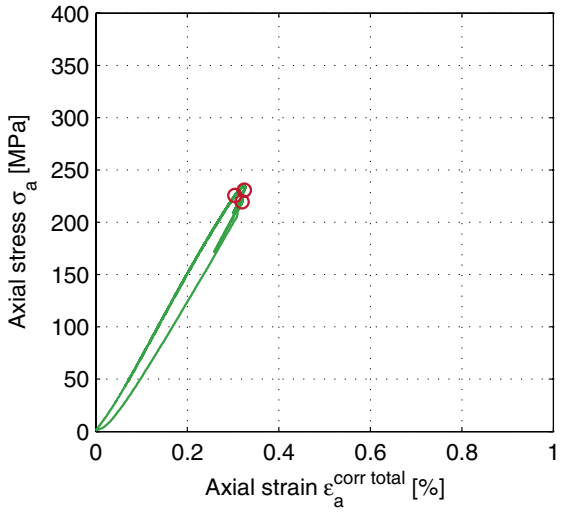

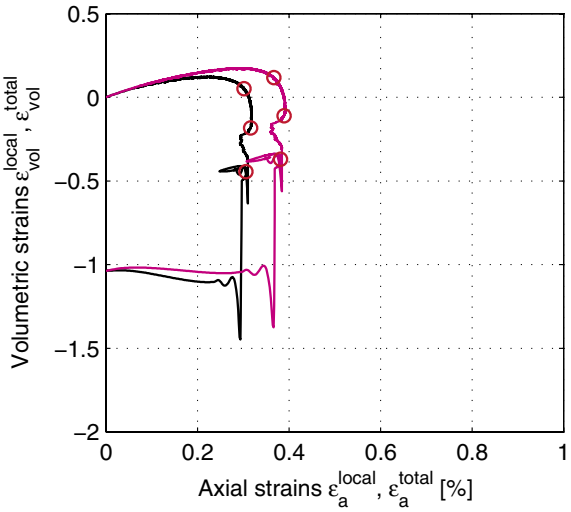

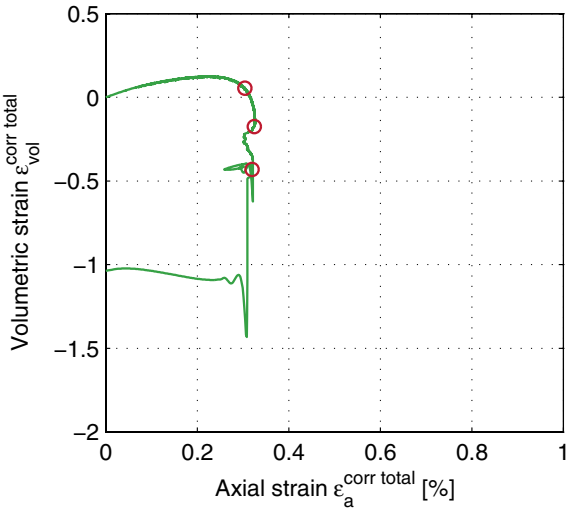

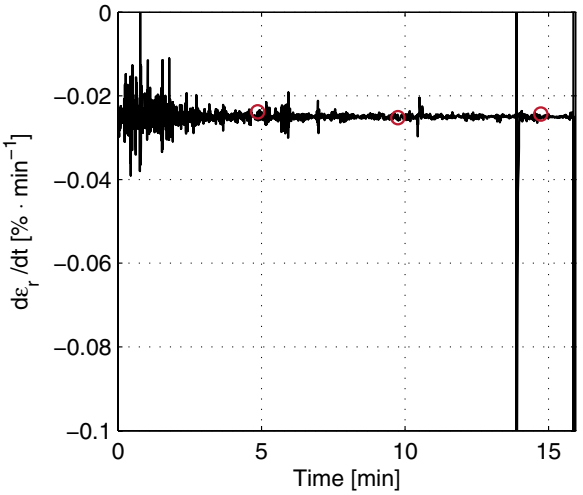

Explanation to curves above:

Based on local deformation (black)

Based on total deformation (magenta)

Based on corrected deformation (green)

Calculated system stiffness:

K_{system} = 5.6333 [GN/m]

Specimen ID: KFM06A–113–18

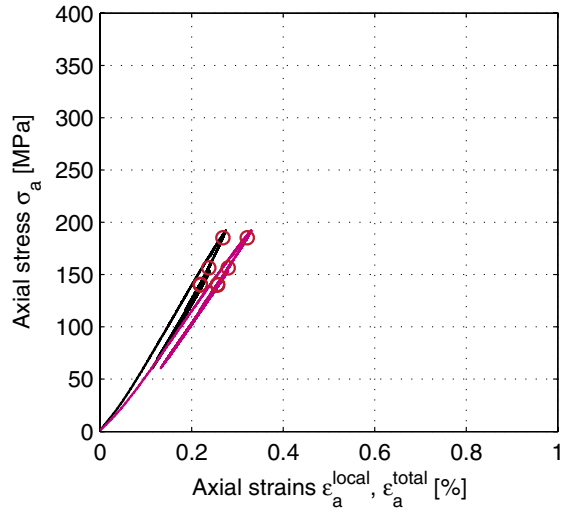

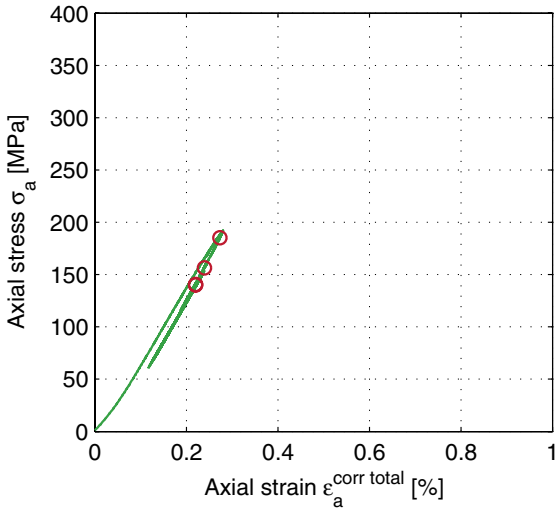

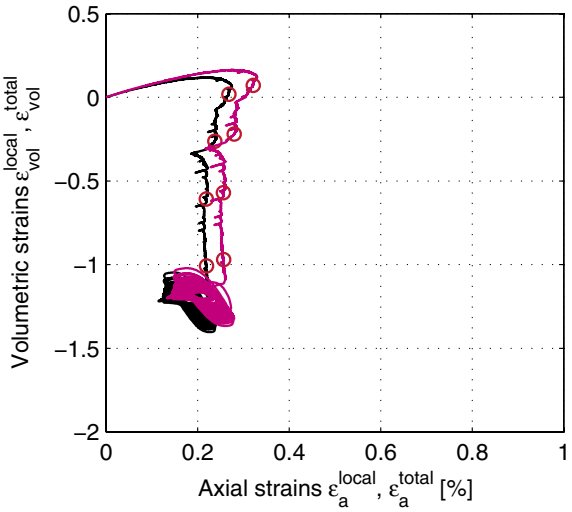

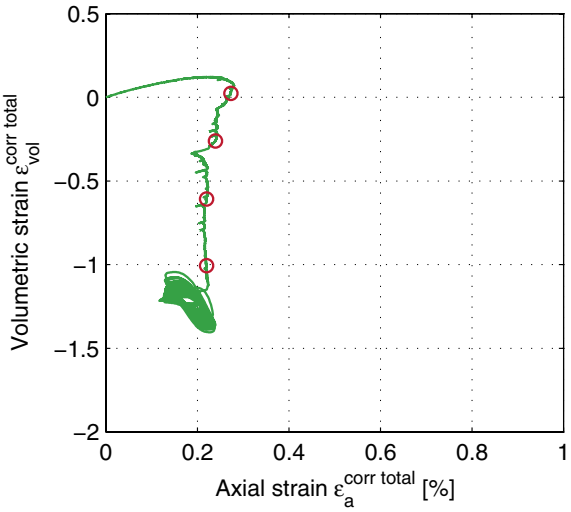

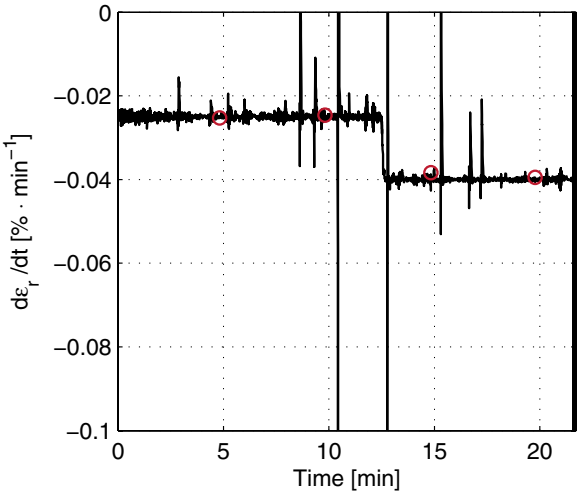

Explanation to curves above:

Based on local deformation (black)

Based on total deformation (magenta)

Based on corrected deformation (green)

Calculated system stiffness:

K_{system} = 6.0436 [GN/m]

Specimen ID: KFM06A−113−19

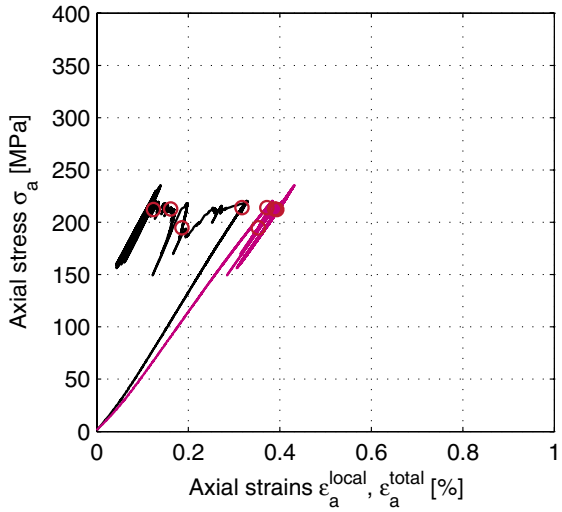

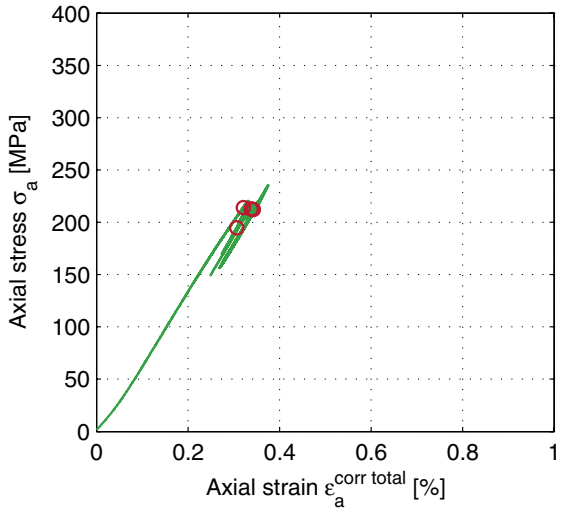

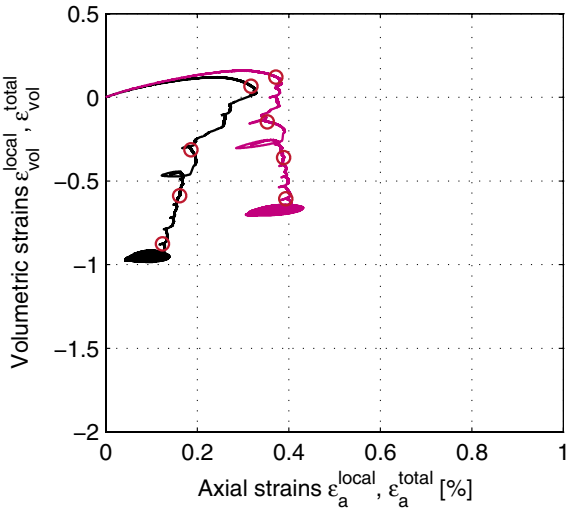

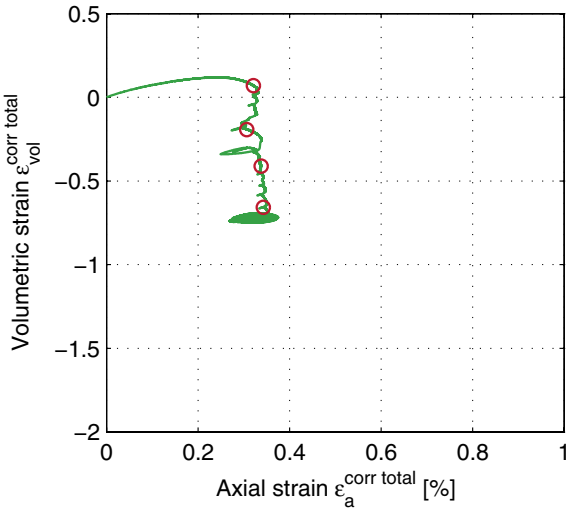

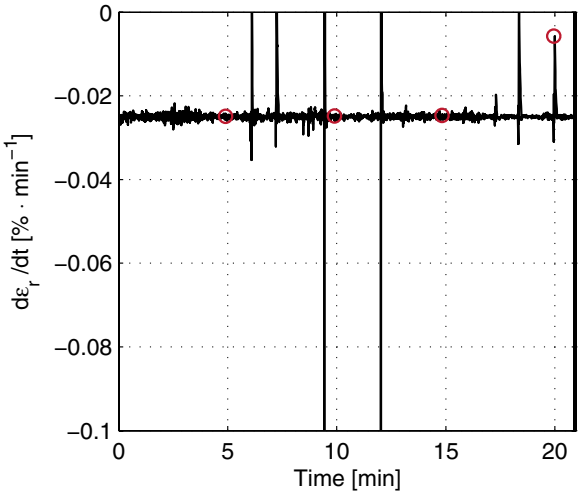

Explanation to curves above:

Based on local deformation (black)

Based on total deformation (magenta)

Based on corrected deformation (green)

Calculated system stiffness:

K_{system} = 6.6186 [GN/m]